Chapter 3

Synthesis and characterization of potassium modified ceria oxide (K-CeO_2), potassium - tin oxide (K-SnO_2), and barium - tin oxide (Ba-SnO_2) catalyst

3.1 Introduction

The present chapter emphasizes the preparation method and various characterizations of three new heterogeneous (mixed metal oxide) catalysts namely potassium modified ceria oxide, potassium tin oxide and barium tin oxide. Potassium modified ceria oxide catalyst was prepared by sol-gel auto combustion method, potassium tin oxide catalyst was synthesized via polymer precursor auto combustion route, and barium tin oxide catalyst was prepared by wet impregnation method. The physicochemical properties of synthesized catalysts were characterized by different techniques. Thermal stability of the catalysts was determined by Thermo-gravimetric analysis (TGA). Phase formation and phase transformation with temperature / time were detected by X-ray diffraction (XRD) analysis. Oxidation states of present elements were identified by X-ray photoelectron spectroscopy (XPS) analysis. Morphological interpretation of the particles and elemental detection were carried out by Scanning Electron Microscope (SEM) – Energy Dispersive X-ray spectroscopy (EDAX). Textural properties were analyzed by Brunauer-Emmett-Teller (BET) – Barrett-Joyner-Halenda (BJH) surface area – pore diameter analyzer. Basic strength or basicity of the catalysts was determined by Hammett indicator titration method.

3.2 Synthesis of Potassium (K) modified Ceria oxide (CeO_2) catalyst

The sol-gel auto combustion was adopted for preparing of potassium modified ceria oxide catalyst. Firstly, the molar ratio of metal nitrates and citric acid was optimized and it was found that 1 : 1.5 was the optimum molar ratio of metal nitrates and citric acid. The precursor nitrates and citric acid were separately dissolved in minimum amount of distilled water. Then, the solution of metal nitrates as poured into the citric acid solution with constant stirring at 80^{o}C. The solution pH was maintained up to 7 by adding 1M ammonium hydroxide solution. At pH 7, the citrate-nitrate complex gets the highest

stability. The complex solution was heated at 110°C. During the heating process ammonia, nitrogen dioxide, carbon dioxide etc were evaporated from the solution mixture which became denser with time. It was ultimately turned into a solid-gel called xerogel. The resultant xerogel was then fired at 250°C. The whole sample was ignited with bright red-yellow flints for 2-3 min, and was converted into fluffy black matter termed as crude catalyst. The crude catalyst was then crushed into fine particles and calcined at different temperatures for 5h in air muffle furnace (Deganello et al., 2009). The final product was stored in a desiccator to prevent from moisture contamination (Zhang et al., 2015).

Following the above preparation method, various catalysts were synthesized varying different variables as per requirements. For the study of catalytic effect of K/Ce atomic ratio in transesterification reaction, a set of catalysts were synthesized varying the K/Ce atomic ratio (1, 1.5, 2, 2.5 & 3); however, to investigate the effect of different calcination temperature, another set of catalysts prepared annealing the crude catalyst at 600, 700, 800, 900 and 1000°C for 5 h. The prepared catalysts were named as xK-Ce oxide Y (x = K/Ce atomic ratio, Y = calcination temperature). For example, the catalyst having K/Ce atomic ratio 2 and calcined at 600°C, was entitled as 2K-Ce oxide 600. The 2K-Ce oxide 800 catalyst was found as the best catalyst for the transesterification reaction. In XRD study, it was found that cerium (Ce) was existed in form of CeO_2 in the catalyst calcined at 800°C. So, especially the catalyst calcined at 800°C named as 2K-CeO_2 800. The synthesis route of 2K-CeO_2 800 has schematically shown in Figure 3.1.

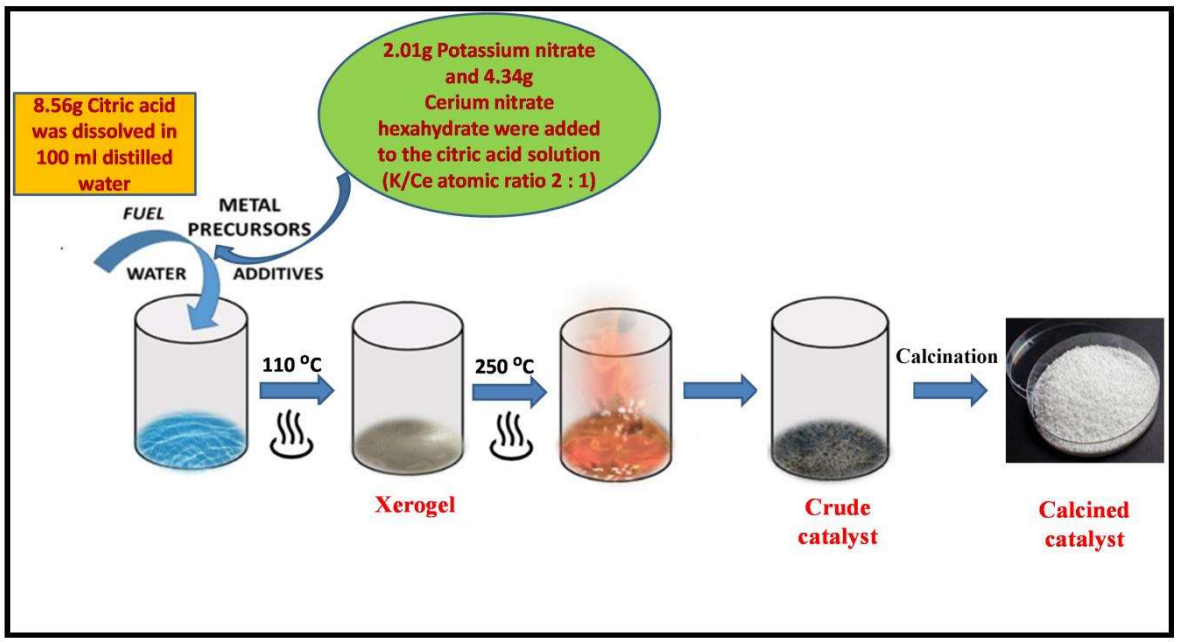

Figure 3.1 Schematic diagram of synthesis route of 2K-CeO_2 800 catalyst via sol-gel auto combustion method

3.3 Characterization of potassium modified ceria oxide catalyst

3.3.1 Thermogravimetric analysis (TGA)

Thermogravimetric analysis (TGA) of pre-calcined K modified ceria oxide is shown in Figure 3.2. The thermal decomposition profile has revealed that four major disintegrations (mass loss) occurred during heat treatment (25^{o}C to 1400^{o}C). The first mass loss of 8.37% at 100^{o}C was corroborated to loss of physisorbed surface water. The second minor weight loss of 2% between 150 to 400^{o}C might have been attributed to the loss of remaining crystal water. A significant weight loss of 11.51% within 400-592^{o}C with a corresponding exothermic peak of 924 mJ/mg in DSC, indicated the complete removal of organic moieties from the sample. Another mass loss of 4.8% between 664-739^{o}C was accompanied by the transformation of Ce_2O_3 and $Ce(OH)_3$ to CeO_2. This fact was further verified by XRD analysis. Another massive weight loss of 23.8% with a sharp exothermic peak of 1.88 J/mg in DSC was observed within 880^{o}C to 1222^{o}C. This might

be related to the volatilization of potassium species (Lahman et al., 1998). The sample showed no further mass loss beyond 1222°C in TGA profile. It means that the K modified CeO_2 catalyst will be thermally stabilized upto 880°C; and it can be anticipated that the optimum activation temperature of the catalyst should have existed between 739-880°C.

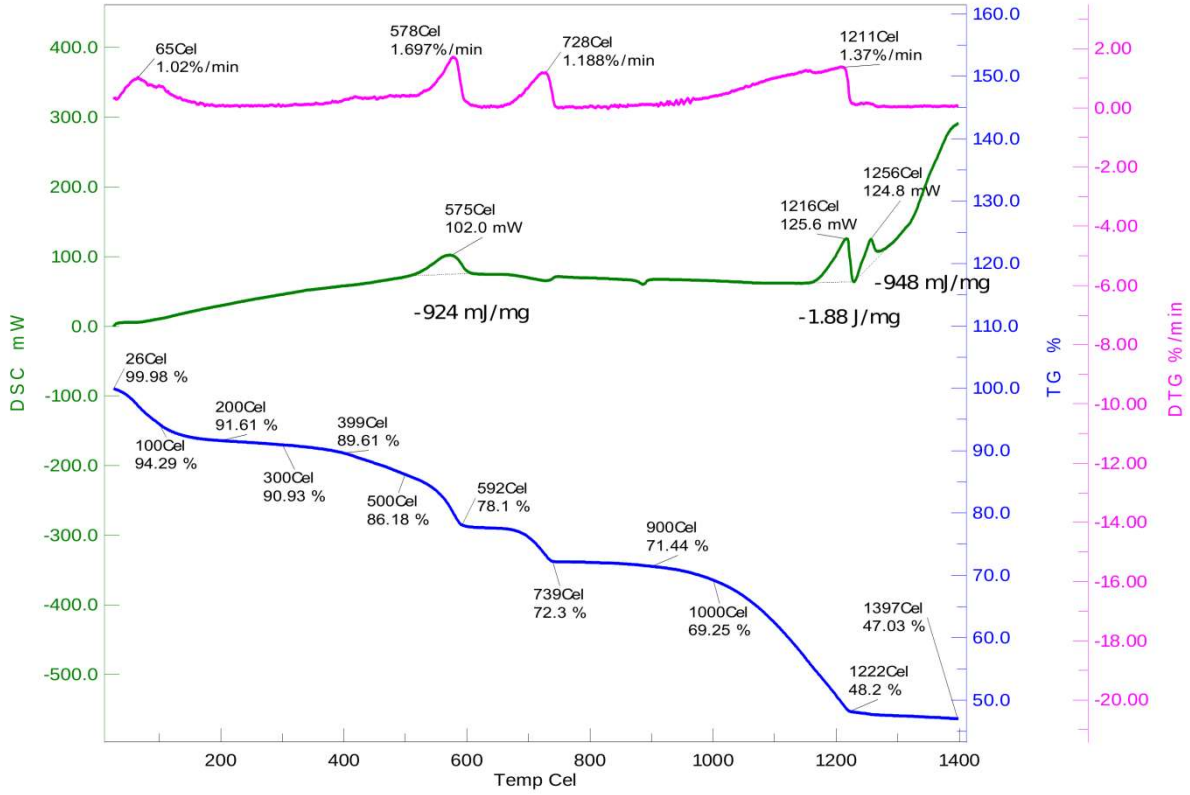

Figure 3.2 TGA-DSC profile of K modified CeO_2 catalyst

3.3.2 Powder XRD analysis

The XRD pattern of cerium oxide activated at 700°C, and 2K-Ce oxides (K/Ce atomic ratio 2) activated at different temperatures such as 600, 700, 800°C are displayed in Figure 3.3. The sharp and intense XRD peaks indicated that the crystalline nature of synthesized cerium oxide as well as 2K-Ce oxides. The characteristic diffraction peaks of cerium oxide activated at 700°C were found at 2θ of 26.4°, 29.5°, 30.3°, 39.9°, 46.6°, 52.8°, 54.4°, 56.1°, 56.6°, 61.1°, 63°, 67.8°, 73.1°, 74.2°, 76°, 80°, 82°, 85°, 86.6°. The diffraction pattern was completely matched with JCPDS file no. 780484, and it represented a

hexagonal structure of Ce_2O_3 with space group P3m1. Similar peak pattern was found in the XRD of 2K-Ce oxide catalysts activated at 600°C and 700°C. This confirmed that cerium was present in 2K- Ce 600 and 2K- Ce 700 catalysts as Ce_2O_3. Additional peaks at 2θ of 15.7°, 27.4°, 28.3°, 39.8°, 48.6° were identified as the distinctive peaks for primitive $Ce(OH)_3$ lattice confirmed by JCPDS file no.740665.

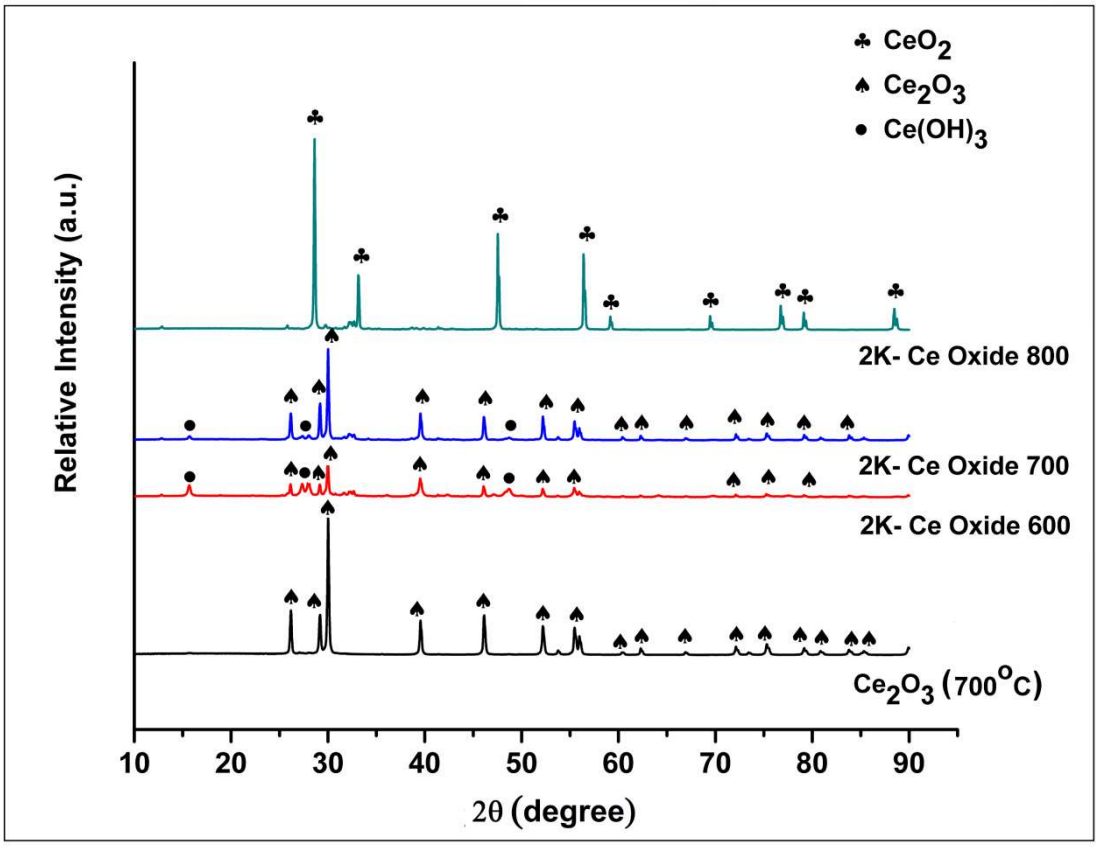

Figure 3.3 Comparative XRD of pure Ce_2O_3 activated at 700°C and K modified Ce oxide catalysts calcined at different temperatures (600, 700, 800°C)

It was also noticed that with increasing activation temperature 600-700°C, the peak intensities corresponding $Ce(OH)_3$ phase were decreased, however, the peak intensities regarding cerium oxide were increased. This suggested that concentration of $Ce(OH)_3$ was decreased and the concentration of Ce_2O_3 was increased at the higher activation temperature. Another interesting fact was also observed in Figure 3.3 that

elevating the catalyst activation temperature from 700°C to 800°C, Ce_2O_3 phase was transformed into a new phase of cerium oxide as the 2K-Ce 800 showed a different peak pattern compared to other two catalysts.

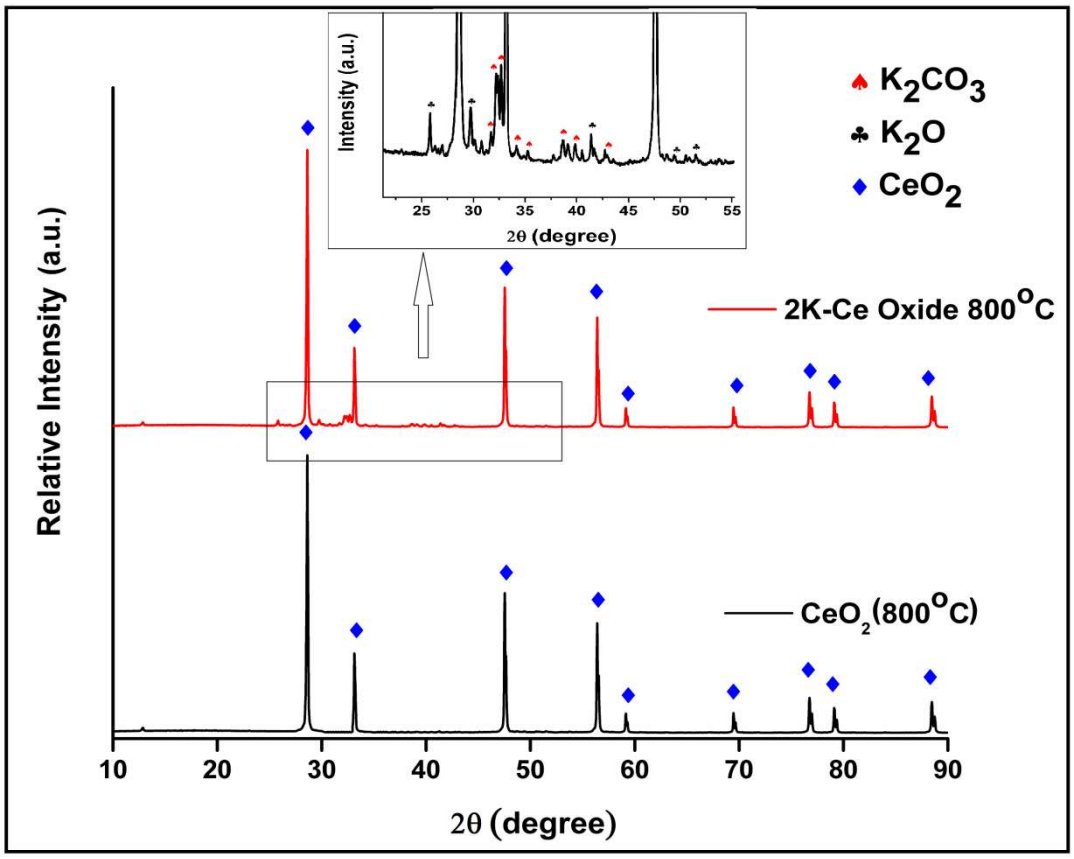

Figure 3.4 Comparative XRD of pure CeO_2 (activated at 800°C) and K modified Ceria oxide catalyst calcined at 800°C (2K-Ce oxide 800)

A comparative XRD pattern of pure CeO_2 (activated at 800°C) and 2K-Ce 800 has been presented in Figure 3.4. The XRD pattern of the catalyst activated at 800°C showed the characteristic peaks of CeO_2, confirmed by matching the peak pattern found at 2θ of 28.5°, 33°, 47.5°, 56.3°, 59°, 69.4°, 76.7°, 79°, 88.4° with the JCPDS file no. 810792 which represents the standard peak pattern for face-centered cubic lattice of CeO_2 (space group Fm3m). The active phases of potassium are shown in the inset of Figure 3.4. It has been found that K_2O and K_2CO_3 were present as the active component of potassium in

2K-Ce 800. The peaks correspond to the 2θ of 25.4°, 29.5°, 41.5°, 51.6°, 49.5° manifested cubic face-centered K_2O lattice (space group Fm3m; JCPDS file no. 772176), however, the peaks at 2θ of 31.7°, 32.1°, 32.7°, 34.1° were obtained for the K_2CO_3 phase (JCPDS file no. 491093). Comparing the XRD of pure CeO_2 and 2K-Ce 800, no peak shifting was observed and also very small intensities of K species were found. This particular fact suggested that successful incorporation and well dispersion of K species into the interstitial position in host CeO_2 lattice during the synthesis process (Yadav et al. 2017).

3.3.3 XPS analysis

Figure 3.5A represents the wide XPS spectra of K modified ceria oxide (2K-CeO_2 800) catalyst. The characteristic peaks of C, K, O, and Ce were found in Figure 3.5A which evidently supported the existence of such elements in 2K-CeO_2 800 catalyst. The C1s spectrum is shown in Figure 3.5B that revealed two intense peaks appeared at the binding energy 284.8eV and 288.5eV for C-C bond in standard C tape and O=C-O bond in carbonate respectively. This also confirmed the presence of carbonate species (K_2CO_3). In the 2p XPS spectra of K (shown in Figure 3.5C), the characteristic binding energy peaks of $K2p_{3/2}$ and $K2p_{1/2}$ were found at 292.6eV and 295.3eV respectively. This ensured the existence of K^+ state in 2K-CeO_2 800 catalyst. In Ce3d spectrum, three pairs of peaks were observed (in Figure 3.5D) for the spin-orbit doublet of Ce^{4+} valence state. Among these six peaks, the set of three peaks of binding energies 883.8eV, 890.7eV and 900eV were assigned for $Ce3d_{5/2}$ spin, and rest three peaks of corresponding binding energy 902.6eV, 909.9eV and 918.2eV were designated for $Ce3d_{3/2}$ spin in CeO_2. This information approved that cerium was present in +4 oxidation state as CeO_2. The 1s spectrum of oxygen (Figure 3.5E) depicted that two different types of oxygen were present in 2K-CeO_2 800 catalyst. The sharp peak at 531.1eV illustrated the existence of

metal – oxygen bond (M-O), however, the broad peak at 532. 4 eV confirmed the presence of physisorbed moisture molecule at the surface of the catalyst.

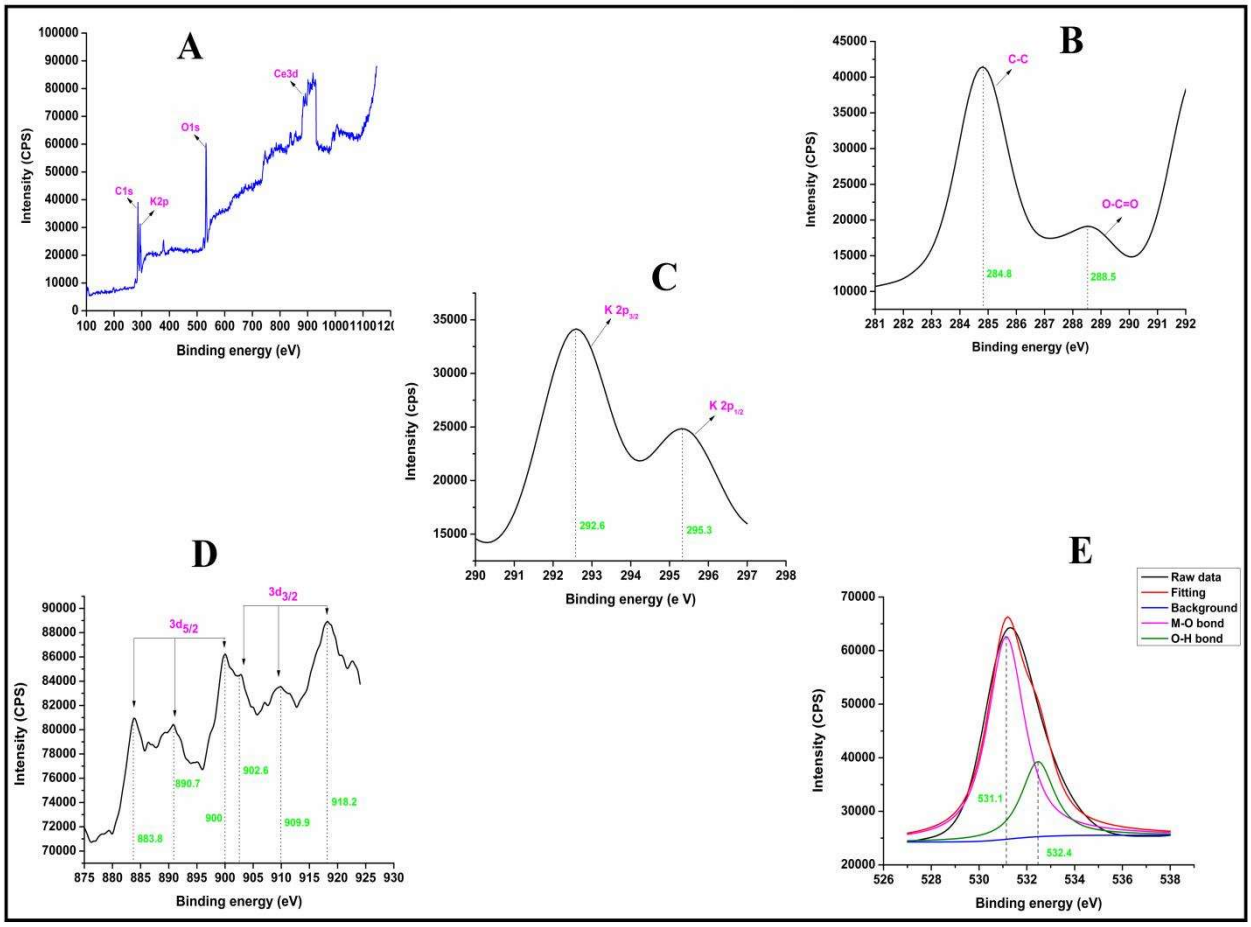

Figure 3.5 A) Wide XPS spectra of 2K-CeO_2 800 catalyst, B) C1s XPS spectra, C) K2p XPS spectra, D) Ce3d XPS spectra, E) O1s XPS spectra

3.3.4 SEM-EDAX analysis

The scanning electorn microscope (SEM) images of ceria oxide (CeO_2) and K modified ceria oxide (2K-CeO_2 800) are represented in Figure 3.6A and Figure 3.6B respectively. The corresponding energy dispersive X-ray (EDAX) diagram of ceria oxide and 2K-CeO_2-800 are displayed in Figure 3.6C and Figure 3.6D. From Figure 3.6A and Figure 3.6B, the topological change of ceria oxide particles after modification was clearly visible. The agglomarated rod shaped ceria oxide was transformed into spherical shaped –

large sized particles of 2K-CeO_2 800. In EDAX of 2K-CeO_2 800 catalyst, the elements K, C, Ce and O were found, which actally supported the XPS results. The K : Ce atomic ratio was found close to the atomic ratio taken in catalyst preparation i.e. 2:1.

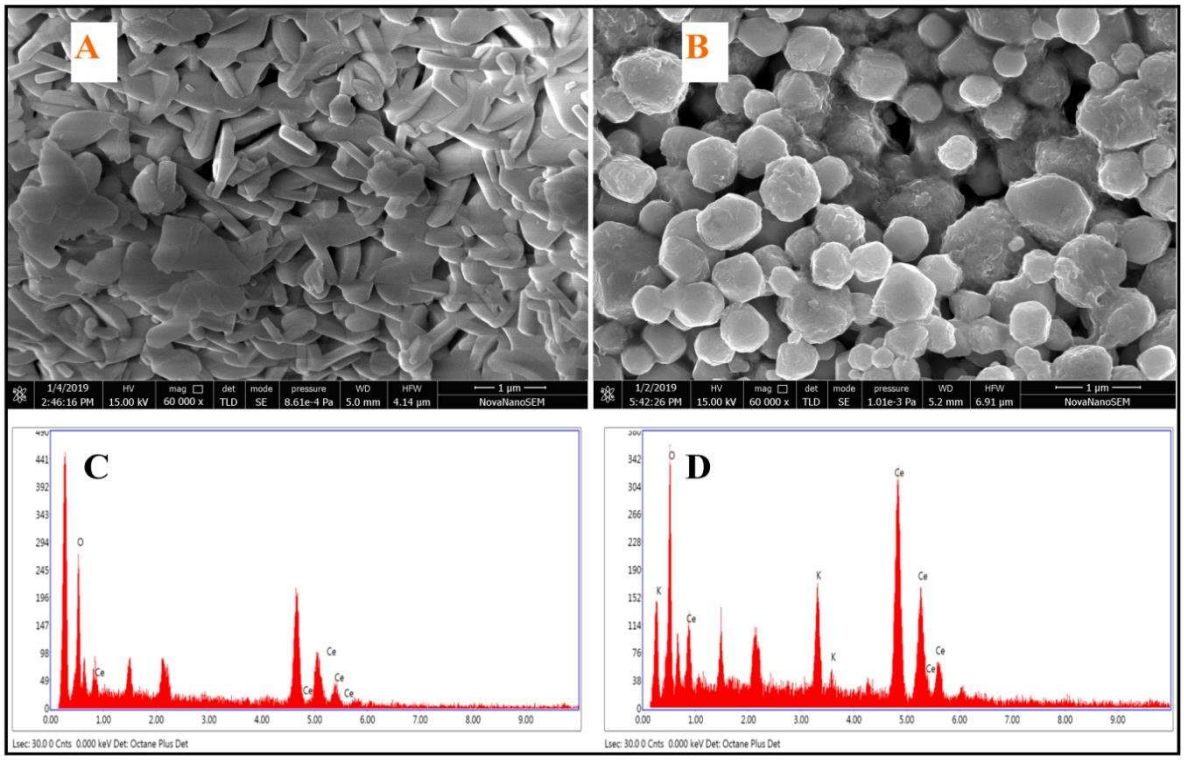

Figure 3.6 SEM image of A) Pure ceria oxide activated at 800°C and B) 2K-CeO_2 800 catalyst; EDAX micrograph of C) Pure ceria oxide activated at 800°C and D) 2K-CeO_2 800 catalyst

3.3.5 BET-BJH analysis

The textural properties like surface area, pore volume and pore diameter of pure ceria oxide and synthesized catalyst (2K-CeO_2-800) were studied by BET nitrogen adsorption-desorption isotherm as shown accordingly in Figure 3.7A and Figure 3.7B. These adsorption isotherms were found to be characteristic type IV with H1 type hysteresis loop. This implied that the materials had mesoporous texture (pore size 2 to 50 nm). The single point surface area and total pore volume of pores of CeO_2 were found to be 5.11m^2/g and 0.0056 cm^3/g respectively. However, the catalyst 2K-CeO_2 800 showed

comparatively low surface area (1.55 m^2/g) and low pore volume (0.0013 cm^3/g). It was expected that after modification by potassium species, the surface area of the catalyst would decrease as the average size of particle increased as shown in SEM images. The pore diameter of the samples was determined by the BJH model from desorption isotherm branch. Figure 3.7C and Figure 3.7D are the BJH plots of pure ceria oxide and 2K-CeO_2 800 catalyst respectively. It was noticed that due to modification of ceria, pore diameter was increased from 6.3 nm to 20.67 nm. Pechimuthu et al. (2007) also observed the similar kind of phenomenon. It was anticipated that the pores of K modified ceria oxide catalyst were interconnected and formed a highly networked pore framework. Also, it was reported that the mesoporous catalyst having a pore size greater than 5 nm showed high efficiency to access the bulky triglyceride molecule (Yadav et al., 2017).

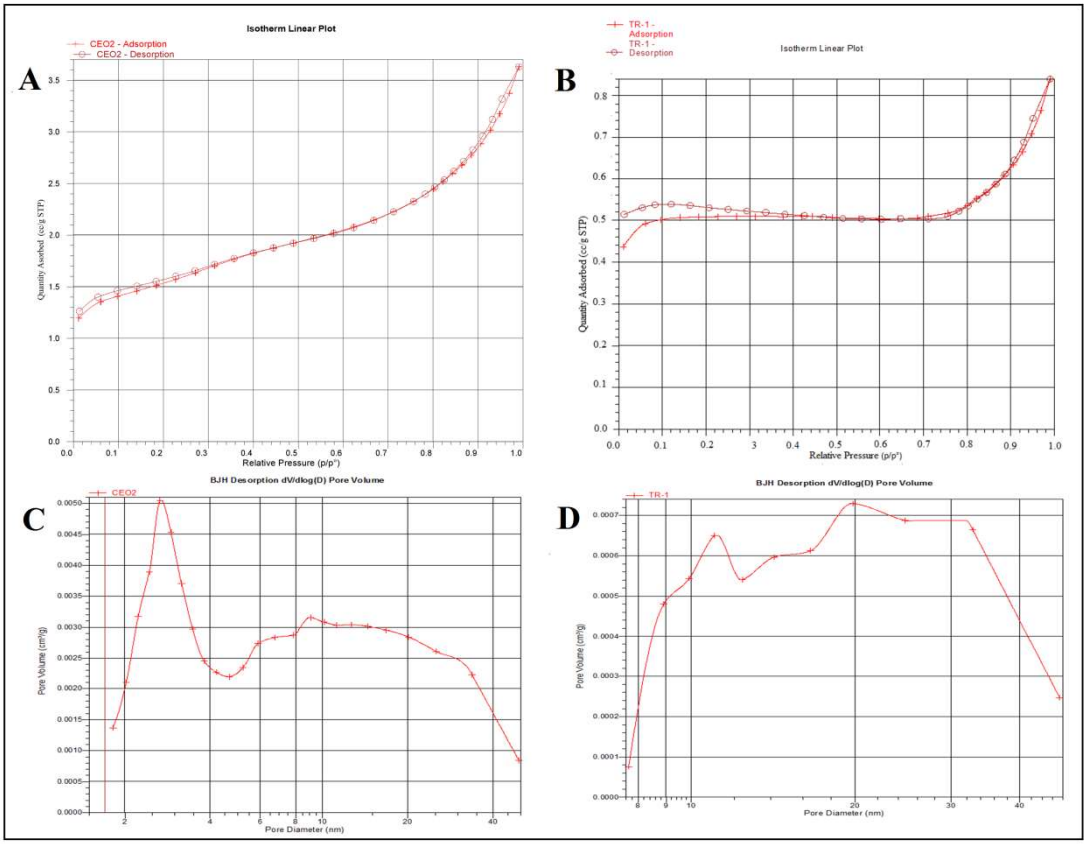

Figure 3.7 Adsorption isotherm of A) Pure CeO_2 and B) 2K- CeO_2 800; BJH plot of C) Pure CeO_2 and D) 2K- CeO_2 800

3.3.6 Basicity analysis

Basicity of the catalyst plays the most important role in transesterification reaction. Basicity of support CeO_2 (pure) and catalyst 2K-CeO_2 800 were evaluated by using Hammett indicator benzene-carboxylic acid titration method. The surface basicity of pure ceria oxide was found in basic strength range of H_ > 7.2. As an appropriate indicator, Bromothymol blue was employed to estimate the basicity of CeO_2, which was found to be 0.55 mmol/g. After modification, basic strength of the catalyst 2K-CeO_2 800 was significantly increased due to incorporation of basic K species into ceria oxide matrix. The basic strength of the catalyst 2K-$CeO_2$800 was subjected between 7.2 < H_< 18.4. There were three indicators namely phenolphthalein, 2.4 dinitroaniline and 4 nitro aniline were selected as Hammett indicators for such basicity evaluation. The cumulative basicity of the catalyst was obtained as a high value of 2.86 mmol/g.

3.4 Synthesis of potassium tin oxide catalyst

The catalyst potassium tin oxide was synthesized in two steps following the polymer precursor- auto combustion method (Sahani et al., 2020) as schematically displayed in Figure 3.8. The first step was tin hydroxide ($Sn(OH)_2$) synthesis by precipitation method. A solution was prepared by dissolving 10g of $SnCl_4.H_2O.5H_2O$ in 100 ml distilled water (DI). Then precipitation of $Sn(OH)_2$ was carried out by adding dropwise 25% ammonium hydroxide into tin chloride solution with the help of a burette under continuous stirring. Ammonium hydroxide was added up to the pH value of the solution 8 to 9, which is the optimum pH for the complete precipitation process of $Sn(OH)_2$. The precipitate was separated from its mother liquor after aging at room temperature for whole day. Then $Sn(OH)_2$ precipitate was washed several times by distilled water to remove the unwanted

chloride ions, followed by drying for 8h at 100°C. A portion of dried $Sn(OH)_2$ was calcined at 800°C for 5h to get the SnO_2 phase for subsequent comparative study.

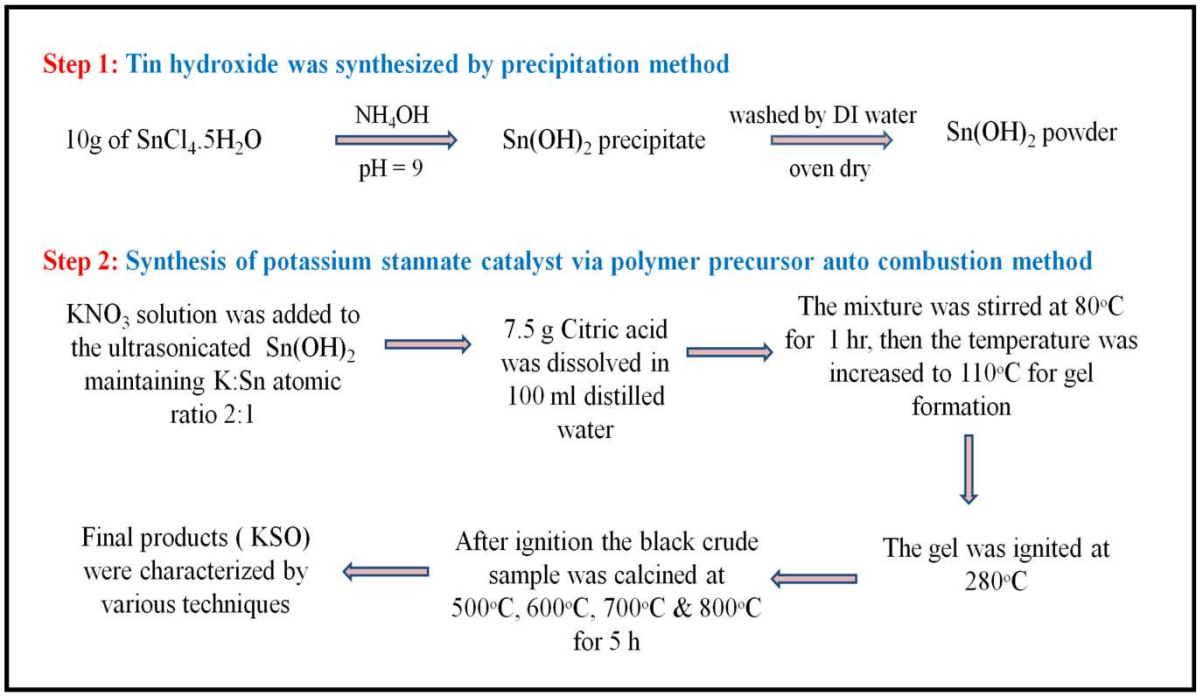

Figure 3.8 Schematic diagram of potassium tin oxide catalyst synthesis method via polymer precursor – auto combustion method

Potassium-tin oxide (KSO) was synthesized in next step (Step 2) as follows. First, a saturated solution of potassium nitrate was prepared by dissolving 2.628 g of KNO_3 in a stipulated amount of water. Then it was poured into ultrasonicated aqueous solution of $Sn(OH)_2$ and stirred for 30 min. K : Sn atomic ratio was maintained as 2:1. Previously prepared aqueous citric acid solution (7.5g in 20ml distilled water) was gradually added to the precursor solution with constant stirring at 65°C. Here the citric acid was used as a complexing agent as well as fuel for the combustion process and it was taken in an equimolar concentration of K and Sn. Thereafter, 25% ammonia solution was added dropwise to the reaction mixture to adjust the pH of the medium 7 which was essential for stabilizing the nitrate-citrate complex (Deganello et al., 2009). Then the

resultant solution was heated at 110°C on a hot plate with continuous stirring at a speeding rate of 400 rpm. Water was continuously evaporated from the reaction mixture which at a time turned to a viscous medium. After 2h of constant heating, the solution mixture became in polymeric (gel) form. Then the resultant gel was fired at 280°C. During the combustion process, the carbonaceous product (i.e. citrate- nitrate complex) was burned with bright yellow flint, citrate was volatilized to CO_2, and nitrates were converted to native oxides of their respective metals. But a small portion of carbon was still present even after completion of the combustion process due to incomplete oxidation. Thus, the product was obtained in form of black floppy residue considered as crude catalyst. Thereafter, the crude catalyst was calcined at four different temperatures: 500, 600, 700 and 800°C (with heating rate 10°C/min) in an air muffle furnace for 5h (holding time). According to their calcination temperature, the activated catalysts were entitled as KSO 500, KSO 600, KSO 700 and KSO 800 correspondingly.

3.5 Characterization of Potassium tin oxide catalyst

3.5.1 Thermogravimetric analysis (TGA)

The thermal decomposition process of crude potassium stannate catalyst has been shown as TGA-DTA profile in Figure 3.9. As can be observed, an initial degradation of 13.54% below 164°C, which was accompanied by three endothermic events, could be relevant for the elimination of adsorbed water and lattice water respectively. Between 184.4°C to 470°C, another mass loss of 5.83% might be resulted due to decomposition of nitrates and citrate. This disintegration was accompanied by formation of metal oxides (SnO_2 and KO_2) and metal carbonate (K_2CO_3). Moreover, this process followed an exothermic pathway which was indicated at 427.6°C in DTA profile. After 480°C, mass loss process occurred in a slow and continuous manner upto 737.4°C. This happened due to

elimination of carbonates (CO_3^2), and was confirmed from the XRD result. Beyond 737.4°C, a sharp degradation in TGA profile was observed between 738°C to 791.7°C. This was accompanied by an endothermic event (found at 771°C in DTA) of phase transformation i.e. individual metal oxides (SnO_2 and KO_2) phases to compound mixed metal oxide phases of potassium stannate. This was also confirmed by XRD analysis. After 791.7°C, the catalyst got the thermal stability up to 846.3°C. However, above 846.3°C, K species started to vaporize in an endothermic process as indicated at 1114.5°C in DTA. So, it is expected that the catalyst will show the best efficacy when it was activated between calcination temperature range 791.7- 846.3°C.

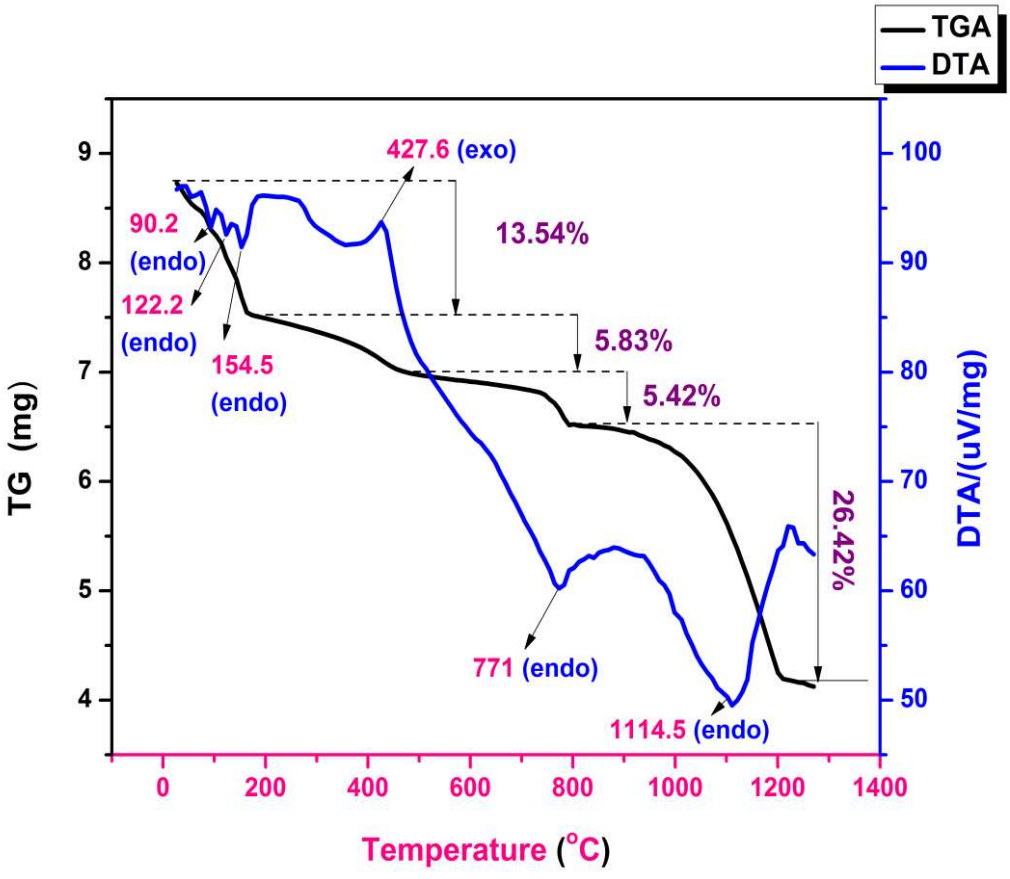

Figure 3.9 TGA-DTA profile of uncalcined potassium tin oxide (KSO) catalyst

3.5.2 Powder XRD analysis

The crystalline phase along with cell parameters of respective lattice arrangement of different KSO sample varying calcination temperature and time was investigated by powder X-Ray diffraction technique. The appeared peaks for a particular crystalline phase, present in diffractogram were confirmed by the help of JCPDS (Joint Committee of powder X-ray diffraction standards) database. Figure 3.10 depicts the diffractogram of KSO catalysts calcined at different calcination temperatures (500,600,700 and 800°C). The diffractogram of KSO 500, KSO 600 and KSO 700 were found to have similar peak pattern, whereas KSO 800 had different pattern. Thus, it can be assured that KSO 500, KSO 600 and KSO 700 possessed same crystalline phase but KSO 800 had different phases.

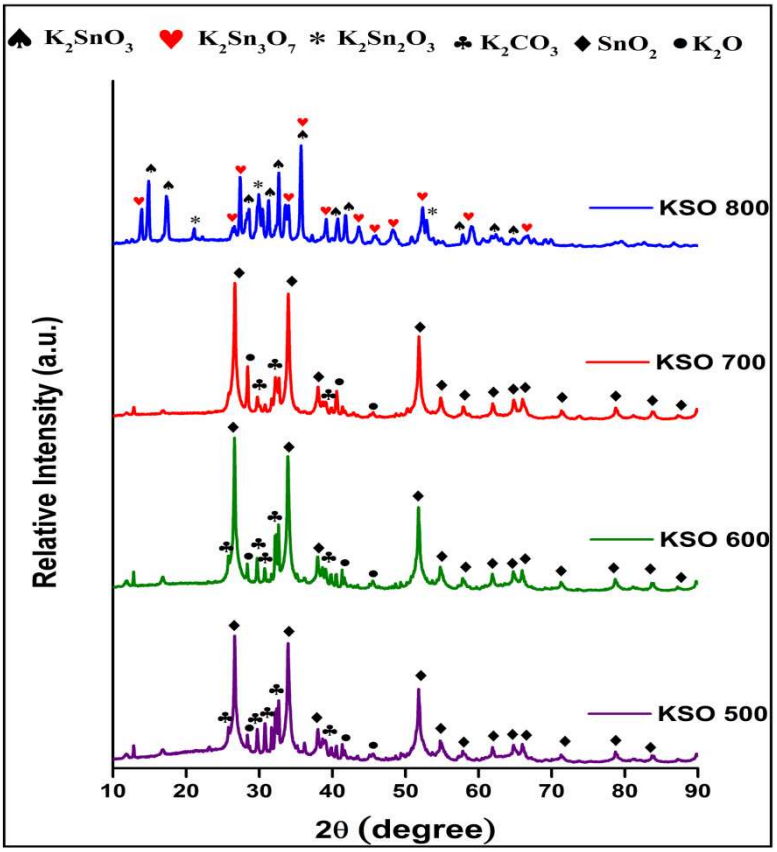

Figure 3.10 Comparative XRD of various KSO catalysts calcined at 500, 600, 700 and 800°C

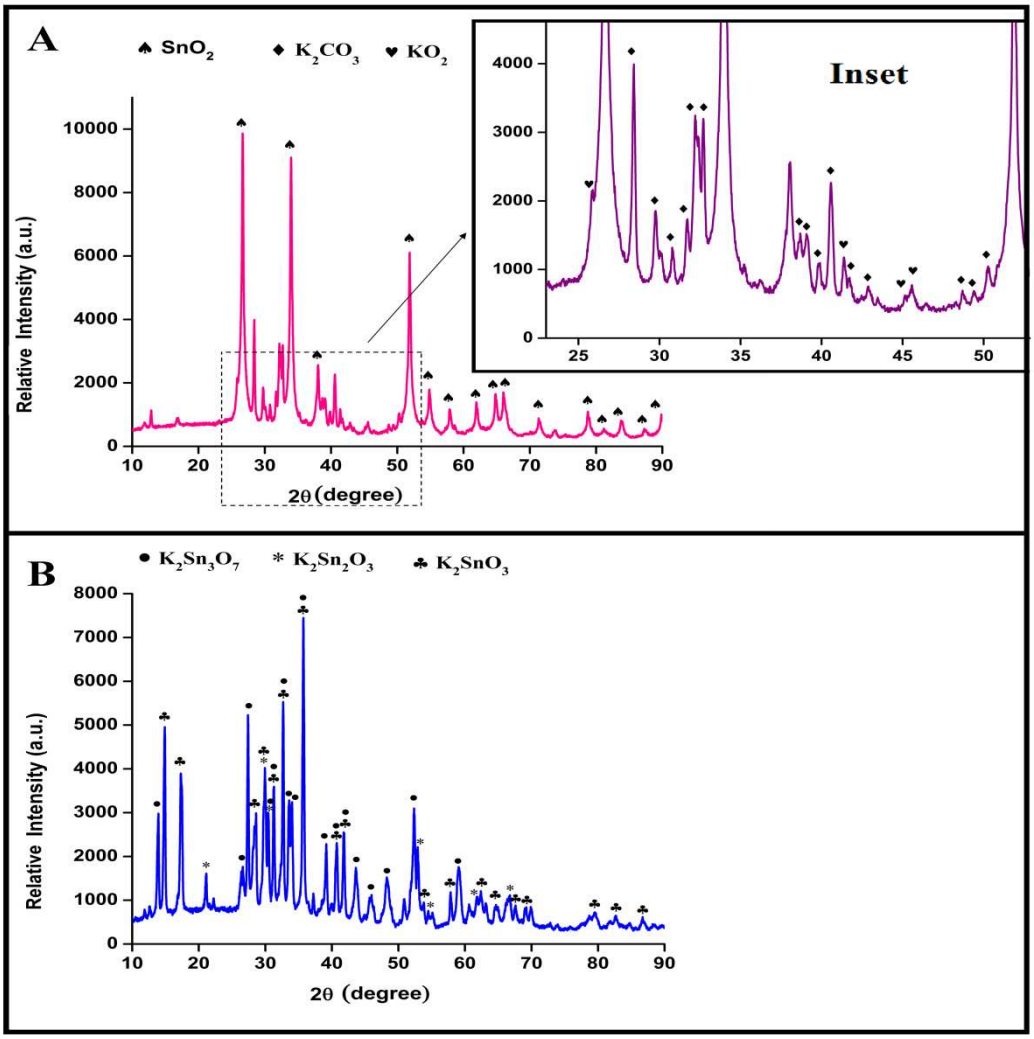

Figure 3.11 XRD of A) KSO 700 (**inset**: the peaks associated with K species between the 2θ values of 25-50^{o} as indicated in XRD of KSO 700) and B) KSO 800

Figure 3.11 shows the characteristic peaks present in XRD diffractogram of KSO 700 and KSO 800. The prominent peaks present in KSO 700 (displayed in Figure 3.11A) were found at the following peak positions as, 2θ = 26.6 (110), 33.9 (101), 37.9 (200), 51.8 (211), 54.8 (220), 57.8 (002), 61.9 (310), 64.7 (112), 65.9 (301), 69.2 (311), 71.3 (202), 78.7 (321), 81.1(400), 87.2 (330), 89.8 (312) were confirmed (by JCPDS file no. 880287) the existence of tetragonal primitive SnO_2 lattice. The peaks corresponding to potassium (K) phases have been displayed in the inset of Figure 3.11A. KO_2 and

K_2CO_3 were found as component phases of potassium in KSO 700 confirmed by JCPDS file no. 895957 and 711466 respectively. Most of the peaks corresponding to the KO_2 were overlapped with the peaks associated with the K_2CO_3 lattice; however, the most intensity peak regarding KO_2 was obtained at 2θ value of 25.8 (110) along with small characteristic peaks at 45 (313), 45.5 (204). The characteristic peaks of monoclinic K_2CO_3 lattice were found at the following 2θ position: 28.7(102), 29.9 (112), 31.7 (130), 32.1 (022), 32.3 (200), 38.6 (202), 39.1 (041), 38.9 (132), 40.6 (013), 41.8 (113), 42.8 (222), 48.8 (300), 49.4 (240), 50.4 (151). Overall it can be concluded that the KSO catalysts activated between 500°C to 700°C possessed SnO_2, KO_2 and K_2CO_3 crystalline phases. Figure 3.11B reveals the crystalline phases present in KSO 800. Three distinct crystalline phases of potassium stannate compound as K_2SnO_3 (# JCPDS file no. 720825), $K_2Sn_2O_3$ (# JCPDS file no. 720196) and $K_2Sn_3O_7$ (# JCPDS file no. 170599) were obtained. Carbonates were completely demolished and formed potassium-tin mixed metal oxides whenever the crude catalyst was calcined at 800°C. This fact of phase transformation was also corroborated the findings in TGA-DTA analysis. All the characteristic peaks of corresponding potassium stannate phases have been pointed in Figure 3.11B. There were also found many peaks of different phases of potassium stannate which were overlapped. Comparing JCPDS database, the peak shifting (±0.5) as well as change in peak intensity was observed but the peak patterns of respective compounds were matched well. The phase transformation of potassium tin oxide catalyst during calcination time at 800°C was also examined and represented in Figure 3.12. This reveals the interesting facts about the effect of high temperature heat treatment (calcination) duration on chemical phase transformation of potassium stannate. Initially (after 1 h), SnO_2 and K_2O were found as the major phase contribution in KSO catalyst. However, no such significant difference in peak intensities was observed even after 2 h,

which means that the aforesaid phases were still existed as major catalytic phases at that period. Then, a remarkable change in intensities was noticed after 3h. The peak intensities corresponding to the SnO_2 and KO_2 phases were decreased; whereas, the assigned peak intensities for potassium stannate phases were increased. This implies that concentration of SnO_2 and KO_2 phases were going to degrade, and the concentration of potassium stannate compounds was enhanced with time. This was continued even after 4 h. After 5 h, the native oxides were completely transformed into potassium stannate compound phase. So, it can be stated that the desirable potassium stannate phases should be evolved by heating the crude sample at 800°C temperature for 5h.

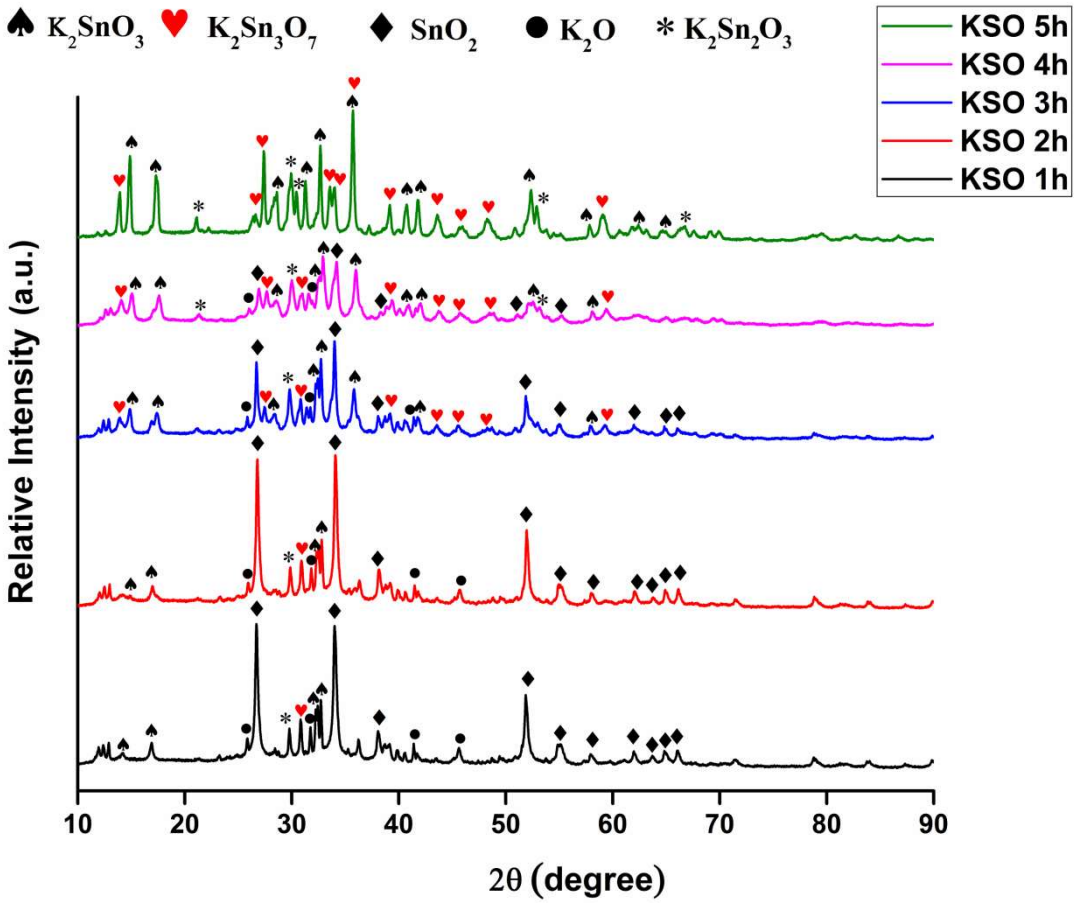

Figure 3.12 Comparative XRD of KSO 800 catalyst calcined for 1, 2, 3, 4 and 5h

3.5.3 XPS analysis

The oxidation state of the elements present in KSO 700 and KSO 800 were investigated by XPS technique. Figure 3.13A and Figure 3.13B depict the wide XPS spectra of KSO 700 and KSO 800 respectively. In both the cases, it was found that K, Sn and O were the constituting elements. However, comparing the X-coordinate i.e. binding energy (BE) of Figure 3.13A and Figure 3.13B, a definite shift in BE for each elements was observed which might have caused by change in oxidation state or change in co-ordination mode (Peuckert, 1985).

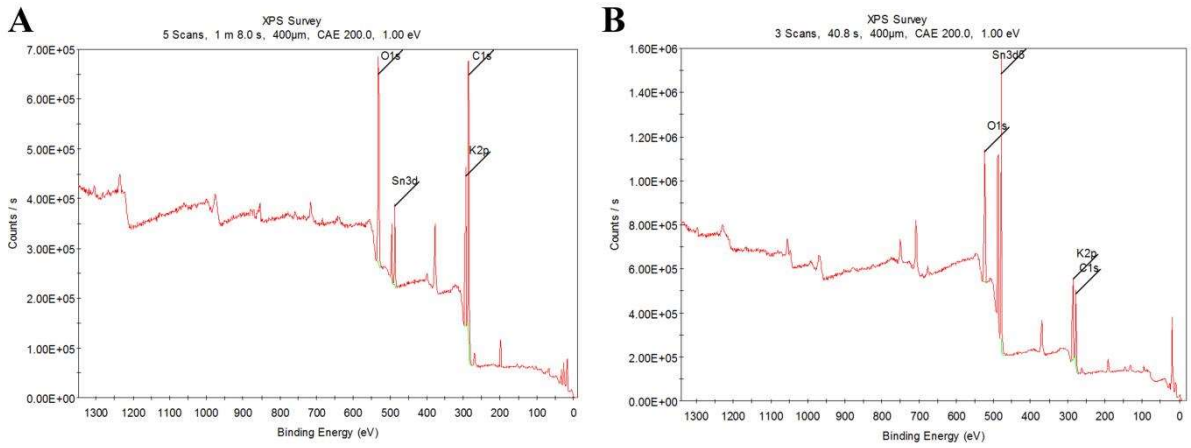

Figure 3.13 Wide XPS spectra of A) KSO 700 and B) KSO 800

Figure 3.14A and Figure 3.14B are C1s spectra of KSO 700 and KSO 800. As can be seen, O=C-O binding energy peak found at 288.1 eV in Figure 3.14A, could be relevant to the carbonate species present in catalyst KSO 700. Figure 3.15A and Figure 3.15B display the 2p spectra of K present in KSO 700 and KSO 800 respectively. The BE of $K2p_{3/2}$ and $K2p_{1/2}$ in XPS of KSO 700 were found at 292.6 eV and 295.4 eV. Spin-orbit components ($K2p_{3/2}$ and $K2p_{1/2}$) were spaced by 2.8 eV, which confirms K^+ state of potassium. However, in XPS of KSO 800, the binding energies of $K2p_{3/2}$ and $K2p_{1/2}$ were

obtained at 292.8 eV and 295.6 eV, which also indicated the +1 oxidation of K. In comparison, the K2p peaks of KSO 800 were shifted approximately to 0.2 eV towards the higher binding energy, which probably happened due to the transformation of K-O bond in KSO 700 to K-O-Sn bond in KSO 800 (Chen et al., 2018).

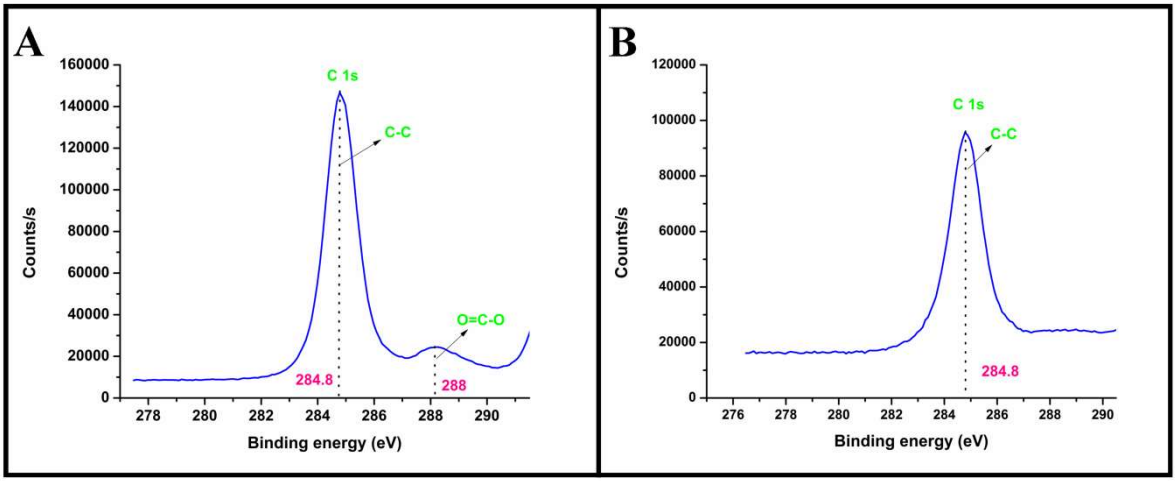

Figure 3.14 A) C1s spectra of KSO 700 and B) C1s spectra of KSO 800

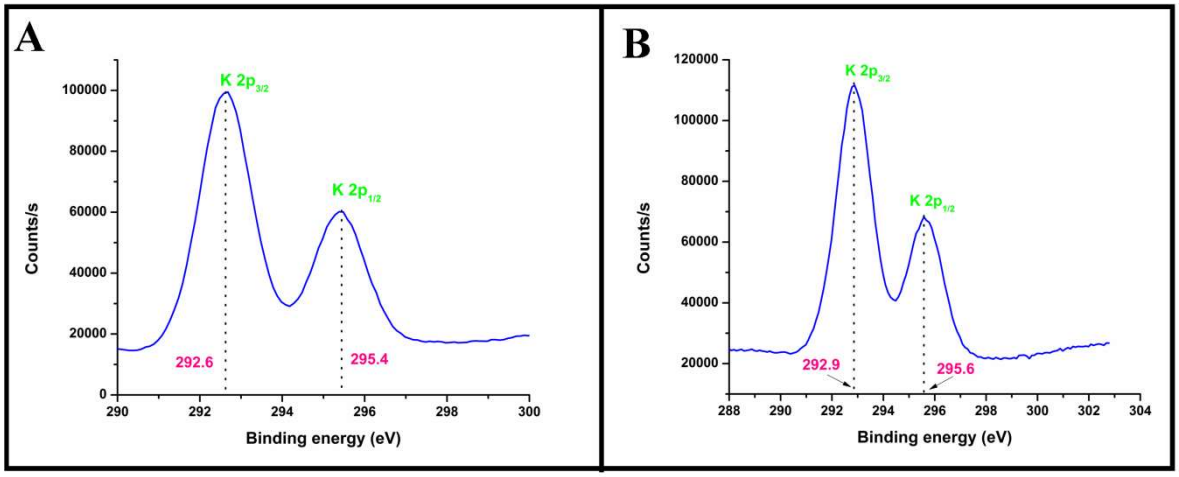

Figure 3.15 A) K2p spectra of KSO 700 and B) K2p spectra of KSO 800

The 3d spectra of tin (Sn) present in XPS of KSO 700 and KSO 800 are shown in Figure 3.16A and Figure 3.16B accordingly. In the case of KSO 700, the corresponding BE of $Sn3d_{5/2}$ and $Sn3d_{3/2}$ were found at 486.7 eV and 495.1 eV, spaced by 8.4 eV. This was assured that Sn was present in +4 oxidation state. Deconvolution of

$Sn3d_{5/2}$ (Figure 3.16C) showed only one best-fitted peak at 486.7 eV; this also reassured that only Sn^{4+} was present as SnO_2 in KSO 700. In case of KSO 800, Sn3d peaks showed a significant shift in BE of 0.6eV towards the lower binding energy. This fact might be associated with the transformation of a definite amount of Sn^{4+} to Sn^{2+}. Our findings are supported by Szuber et al. (2001). Deconvolution of Sn $3d_{5/2}$ (Figure 3.16D) showed two peaks corresponding to two oxidation states of Sn present in KSO 800. The peak at lower BE (485.7 eV) was assigned for Sn^{2+} and the higher BE (486.4 eV) peak was designated to Sn^{4+} (Jadhav et al., 2017, Kwoka et al., 2005).

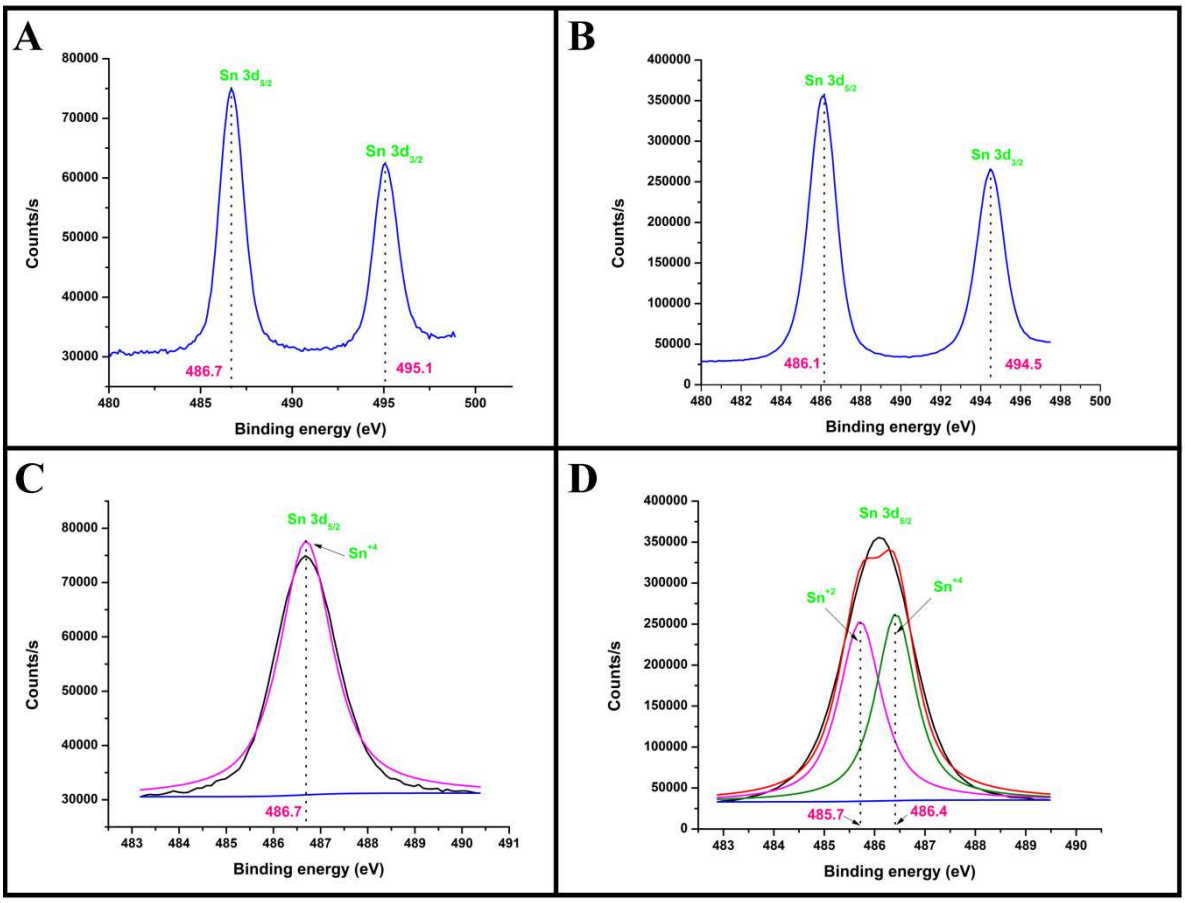

Figure 3.16 A) Sn3d spectra of KSO 700, B) Sn 3d spectra of KSO 800, C) deconvolution of $Sn3d_{5/2}$ of KSO 700 and D) deconvolution of $Sn3d_{3/2}$ of KSO 800

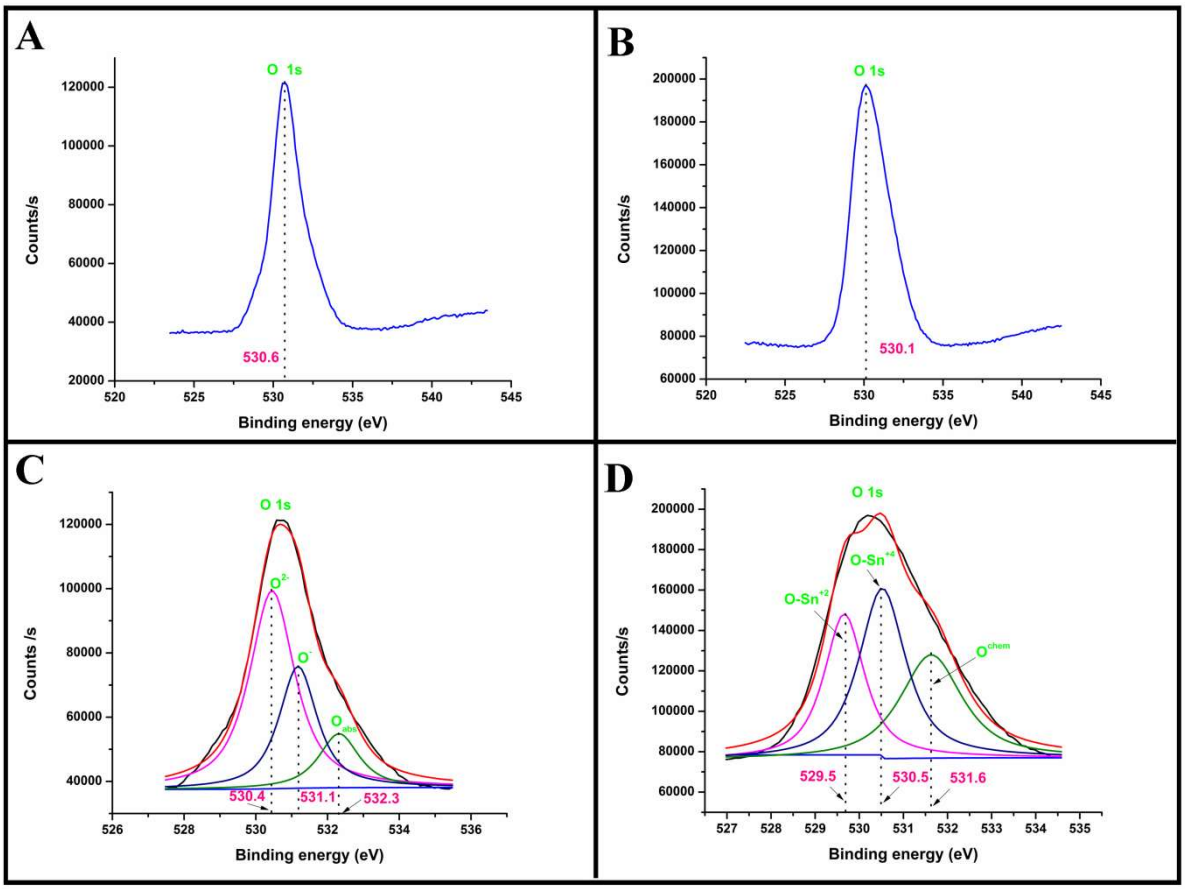

Figure 3.17 A) O1s spectra of KSO 700, B) O1s spectra of KSO 800, C) deconvolution of O1s of KSO 700 and D) deconvolution of O1s of KSO 800

The BE associated with the O1s of KSO700 and KSO 800 were found at 530.6 eV and 530.1 eV from Figure 17A and Figure 17B respectively. Here also, a lower shift of 0.5 eV in O1s spectra for KSO 800 was noted. This result corroborated the fact delivered for Sn. Due to the transformation of O-Sn^{4+} to O-Sn^{2+} with increasing calcination temperature 700°C to 800°C, both Sn and O showed lower binding energy shifts (Jadhav et al., 2017). The deconvolution of O1s in XPS KSO 700 (Fig 5C) revealed three peaks were present under the singlet O1s peak; one at 530.4 eV assigned to metal oxide (O^{2-}), the second at 531.1 eV indexed to superoxide O (O^{-}) present in KO_2, and the last one at 532.3 eV assigned to the physically adsorbed O which might come from

moisture content present at the outer surface of the catalyst. In XPS of KSO 800, the deconvolution of O1s (Figure 3.17D) also depicted presence of three peaks for three different types of O. The lowest BE peak at 529.5 eV was subjected to the O of O-Sn^{2+}, the middle one at 530.5 eV was designated O of O-Sn^{4+}, and the higher one at 531.6 eV was assigned to the chemically adsorbed O on the catalyst surface (Wu et al., 2015). Therefore, the XPS analysis of KSO catalysts confirmed the transformation of tin oxide and potassium oxide to potassium stannate with increasing calcination temperature 700°C to 800°C, as well it helped to cross-verify the XRD data.

3.5.4 SEM-EDAX analysis

The surface topology of tin oxide and potassium tin oxide catalysts (KSO 700 and KSO 800) was visualized by SEM technique. Figure 3.18 depicts the morphological difference in three samples namely pure SnO_2, KSO 700 and KSO 800. Besides, the elemental analysis was carried out by the EDAX technique and has been shown accordingly. It has been clearly seen in Figure 3.18A that pure SnO_2 had no particular shape and size; moreover, agglomeration of particles and heterogeneity in size distribution implied the amorphous character of SnO_2. The component phases present in KSO 700 has been displayed in Figure 3.18B. Comparing Figure 3.18A and Figure 3.18B, it can be better understood that how the layer of K species covered the whole SnO_2 surface. Small spherical shaped KO_2 and K_2CO_3 species were irregularly deposited over SnO_2 particles. This was due to the strong philicity of K-O bond of K- species toward the Lewis acidic sites (Sn^{4+}-O) present on the surface of SnO_2. Figure 3.18C shows the surface morphology of catalyst KSO 800 where three different types of particles such as rod-shaped particles, the dull shaded amorphous solid of large particles, and the agglomerated spherical shaped particles were spotted.

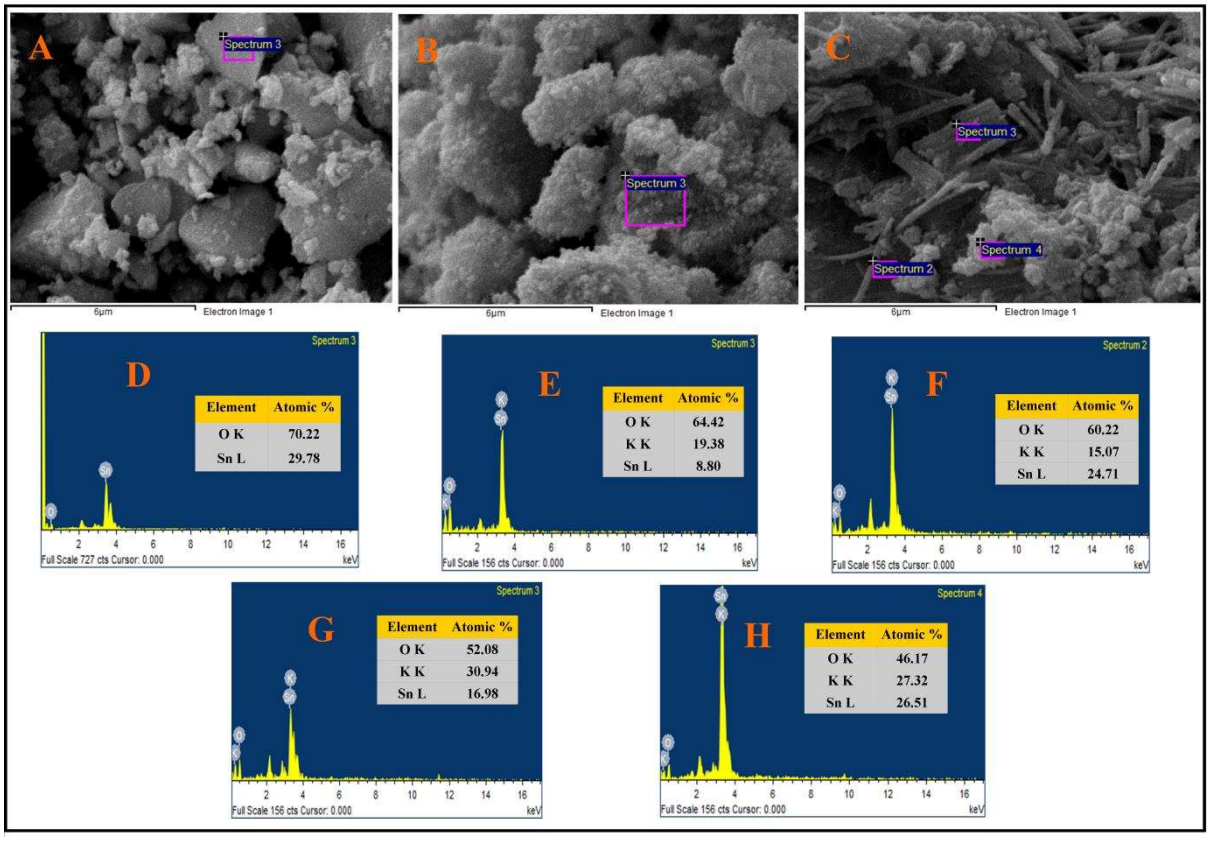

Figure 3.18 SEM image of A) Pure SnO_2, B) KSO 700 and C) KSO 800*; EDAX micrograph of D) pure SnO_2, E) KSO 700, F) KSO 800 (spectrum 2), G) KSO 800 (spectrum 3), H) KSO 800 (spectrum 4)**

*All the areas / points chosen for EDAX analysis mentioned in corresponding SEM images

**Insets of the EDAX include the atomic weight (%) of existing elements

The identification of phases present in the sample was carried out by EDAX analysis of a particular area or point (mentioned in Figure 3.18A, Figure 3.18B and Figure 3.18C) as required. The EDAX micrograph of such respective areas or points has been introduced as Figure 3.18D for pure SnO_2, Figure 3.18E for KSO 700 and Figure 3.18F to Figure 3.18H for KSO 800 with atomic weight (%) of elements which describes the possible atomic ratio of the elements and the molecular formula of the existing phases. In the case of pure SnO_2, the obtained atomic weight (%) of O : Sn was around 2 : 1, which suggested that the existing phase was SnO_2. Similarly, in KSO 700 catalyst showed K : Sn atomic ratio around 2 : 1 which was approximately the same ratio that was taken in

catalyst preparation. Then the point EDAX of KSO 800 helped to interpret the topology of chemically different potassium stannate phases i.e. rod shaped particles were of K_2SnO_3, large sized particles were of $K_2Sn_3O_7$, and agglomerated spherical particles were of $K_2Sn_2O_3$. Such EDAX data was also perspicuously supported the facts explained earlier in XRD and XPS analysis.

3.5.5 BET-BJH analysis

The solid-base catalyzed transesterification reaction is mainly driven by two physicochemical properties of catalyst; one is surface area and the other is basic strength. Basically, the process is synergistically actuated by both the aforementioned factors. The change in surface property due to increase in calcination temperature of potassium stannate catalysts have been presented in Table 3.1. Pore sizes of all KSO catalysts were obtained in the range of mesoporous material (i.e. 2-50 nm). Surface area of KSO 500, KSO 600 and KSO 700 possessed lower surface area; however, a slight increase in surface area was also observed with increasing calcination temperature. KSO 800 showed the best surface properties among all the potassium tin oxides. These facts can be explained with the help of XRD and SEM analysis. Previously we found in XRD that the peak intensities associated with carbonates were reduced accordingly with enhanced calcination temperature from 500^oC to 700^oC, and it was completely demolished at 800^oC. The SEM image of KSO 700 revealed that carbonates were heterogeneously accumulated onto the SnO_2 surface, which was the definite cause of surface area reduction. So, it can be anticipated that the concentration of carbonate species decreased with increasing calcination temperature, as a consequence, the surface area of catalysts increased accordingly. KSO 800 was composed of carbonate-free pure potassium stannate compounds that were morphologically far better compared to other KSO catalysts . Thus, it showed the best result in BET surface area analysis also.

Table 3.1 Surface properties of potassium tin oxide (KSO) catalysts

Name of the sample	Surface area (m^2/g)	Pore volume (cm^3/g)	Pore size (nm)
KSO 500	0.86	0.0047	18.34
KSO 600	1.78	0.0066	23.94
KSO 700	5.65	0.0094	28.56
KSO 800	32.04	0.0558	15.09

3.5.6 Basicity analysis

The basic strength of the catalysts was measured by Hammett indication benzoic acid titration method. The basicity of KSO 500, KSO 600, KSO 700 and KSO 800 was found to be 0.77 mmol/g, 0.97 mmol/g, 1.21 mmol/g and 1.76 mmol/g respectively. The basic strengths of such KSO catalysts were exhibited between the pK_a= 7.9 to 9.5. So, phenolphthalein was used as indicator for the titration. Here also, we can see that basicity was improved with enhancing calcination temperature. Basically, carbonate (CO_3^{2-}) is acidic in nature and it usually clogged the basic active sites. In XRD analysis, it was found that the concentration of carbonate species was decreased with increasing calcination temperature. So, at higher temperatures, the acidic carbonates were removed from the basic sites of the catalyst surface which consequently improved the basicity (Sahani et al. 2019). KSO 800 demonstrated the best result in basicity due to the complete elimination of carbonate species from its surface. So, considering surface properties and basicity, KSO 800 was approved as the best catalyst among other KSO catalysts for biodiesel production from waste cooking oil and castor oil via transesterification process.

3.6 Synthesis of barium tin oxide catalyst

The barium tin oxide catalyst was prepared by wet impregnation of tin hydroxide into barium nitrate solution, schematically shown in Figure 3.19. At first, barium hydroxide was prepared by precipitation method. The required amount of tin (IV) chloride pentahydrate ($SnCl_4.5H_2O$) was dissolved in 50 ml distilled water. Then 25% ammonia solution was added dropwise to the tin chloride solution under constant stirring up to the pH value 9. After ensuring the complete precipitation of tin hydroxide, the white slurry mixture was left under constant agitation for 1 day. The day after, precipitate was separated from the mother liquor by vacuum filtration and washed several times by distilled water to remove the chloride ion and other impurity ions. Then, prepared $Sn(OH)_2$ precipitate was dried overnight in hot air oven at 110^oC, followed by crushing into fine particle of $Sn(OH)_2$. Pure tin oxide (SnO_2) was prepared by calcining tin hydroxide at 850^oC for 5h in air muffle furnace. The solid barium tin oxide catalysts with different Ba/Sn atomic ratios (1 : 1, 2 : 1, 1 : 2) were prepared by impregnating $Sn(OH)_2$ powder into a saturated barium nitrate solution. In typical $BaSnO_3$ preparation, 1 g of $Sn(OH)_2$ powder was impregnated into the aqueous solution of 1.21g $Ba(NO_3)_2$. The mixture was agitated at 80^oC to get its slurry form. Then it was dried at 110^oC for overnight in an air oven. The obtained solid product was finely crushed and calcined at 850^oC in an air muffle furnace for 5h (Xie and Zhao, 2013). The synthesized barium tin oxide samples having different Ba : Sn atomic ratio, designated as BSO (Ba : Sn = 1 : 1), 2BSO (Ba : Sn = 2 : 1), B2SO (Ba : Sn = 1 : 2), were characterized by various techniques as mentioned below.

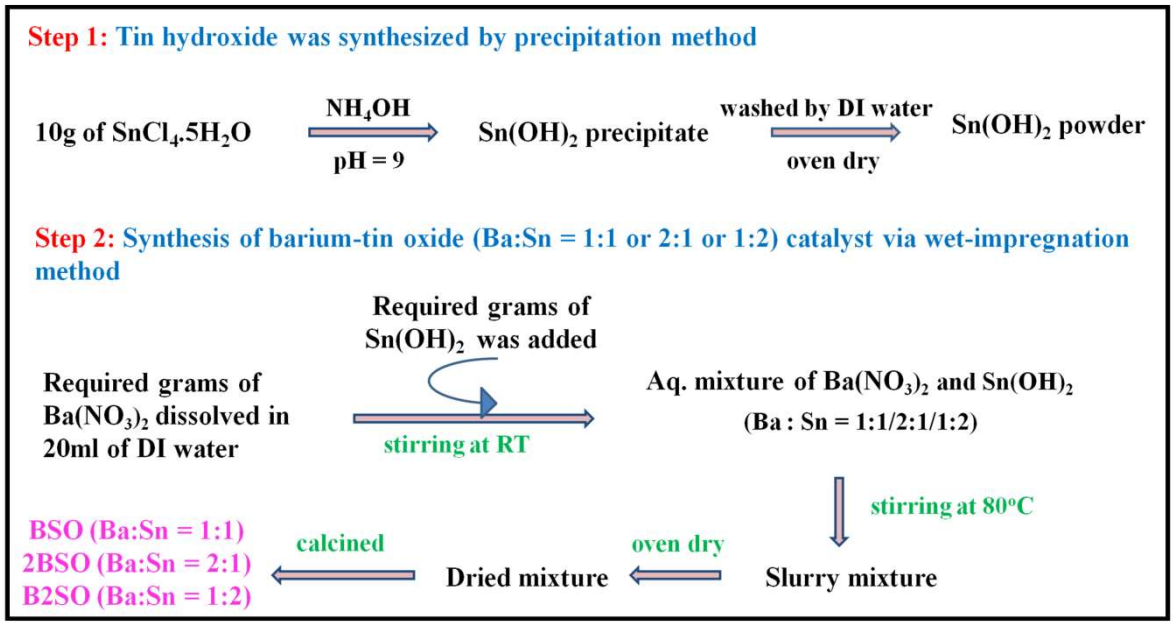

Figure 3.19 Schematic diagram of barium tin oxide catalyst preparation via wet impregnation method

3.7 Characterization of barium tin oxide catalyst

3.7.1 Thermogravimetric analysis (TGA-DTA)

The thermal disintegration profile of the uncalcined barium stannate (Ba : Sn = 1 : 1) sample has been shown in Figure 3.20. It was observed that during the heat treatment process (35 to 1000°C), total ~40% mass loss occurred in two events. Initially, 4% mass loss was appeared up to 400°C due to elimination of physically adsorbed surface water and the crystalline water. Aftermath, 36% mass loss was taken place between 400°C to 758°C, which was accompanied by two corresponding endothermic DTA peak around 590°C and 685°C assigned for decomposition of barium nitrate and tin hydroxide respectively. Thus, it can be depicted that this major mass loss is associated with $BaSnO_3$ formation from the respective precursor moieties i.e. nitrates and hydroxides (Roy et al., 2018). After 758°C, no mass loss was found up to 1000°C in TGA profile. This means the

catalyst became thermally stable at a calcination temperature of 758°C. So, it is anticipated that the optimum activation temperature of barium stannate would be greater than 758°C.

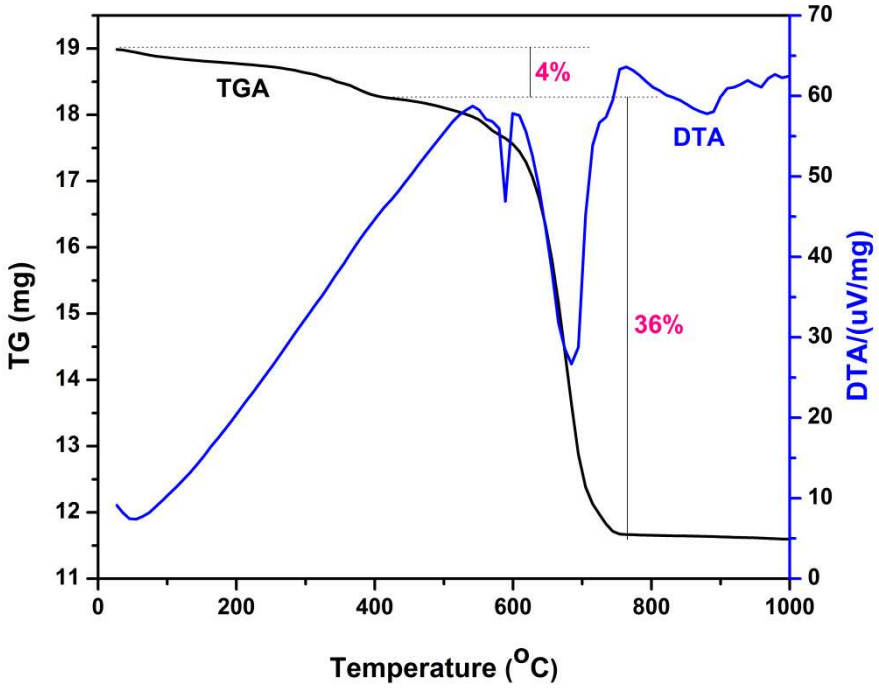

Figure 3.20 TGA-DTA profile of uncalcined barium tin oxide catalyst

3.7.2 Powder XRD analysis

The prepared catalyst samples (BSO, 2BSO, B2SO) were characterized by powder XRD to find out the phases formed into the materials. The relative diffractogram (Figure 3.21A) has implied the impact of different Ba/Sn atomic ratio on chemical phase formation in barium tin oxide catalysts. The XRD pattern of SnO_2 powder had no sharp peak indicating the complete amorphous state of tin oxide. The major XRD peaks of the barium tin oxides (BSO, 2BSO, B2SO) positioned at 2θ (hkl) = 30.7° (110), 37.9° (111), 44° (200), 54.6° (211), 64° (220), 72.7° (013), 81° (222), 89° (123) were assigned as characteristic peaks of primitive cubic lattice of $BaSnO_3$, confirmed by JCPDS file no.

741300 (Wu et al., 2012). BSO had pure $BaSnO_3$ phase, however, 2BSO (Ba/Sn 2:1) and B2SO (Ba/Sn 1:2) had $BaSnO_3$ along with additional phase of stoichiometrically excess component. Ba was present in excessive amount in 2BSO; however, Sn was in excess in B2SO. Such excess Ba in 2BSO existed in form of $BaCO_3$ phase (JCPDS file no. 712394), whereas, excess Sn in B2SO was present in form of SnO_2 (JCPDS file no. 880287).

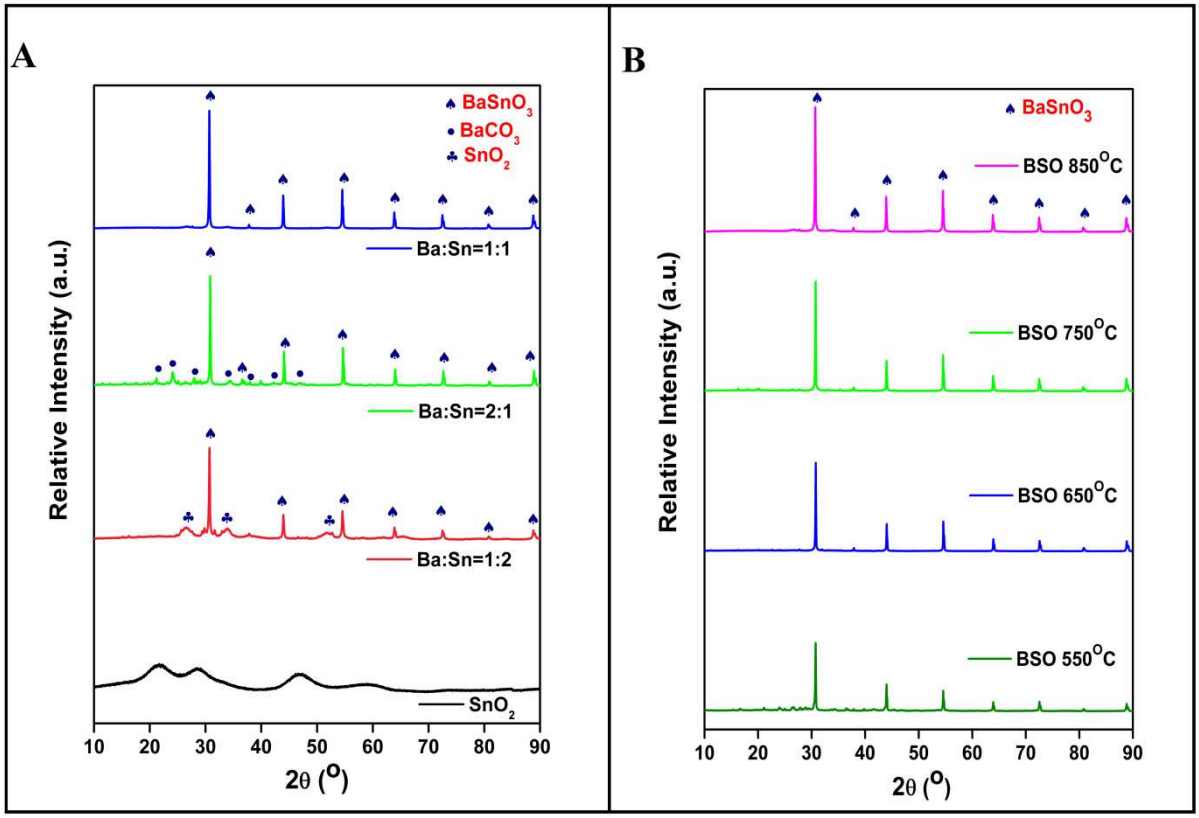

Figure 3.21 A) Comparative XRD of pure tin oxide and barium tin oxides (BSO, 2BSO, B2SO) and B) comparative XRD of BSO catalysts calcined at 550°C, 650°C, 750°C, and 850°C

A scrutiny on catalyst calcination temperature was performed to investigate the impact of high temperature on phase formation of BSO catalyst. Figure 3.21B has manifested that BSO got pure $BaSnO_3$ phase at the calcination temperature of 550°C but the phase became more prominent and highly intense at 850°C. This result

substantiates the TGA result which primarily gave an idea about the activation temperature which might be greater than 758°C.

3.7.3 XPS analysis

Elemental composition and the oxidation state of the constituent elements present in BSO catalyst (calcined at 850°C) were detected by XPS analysis.

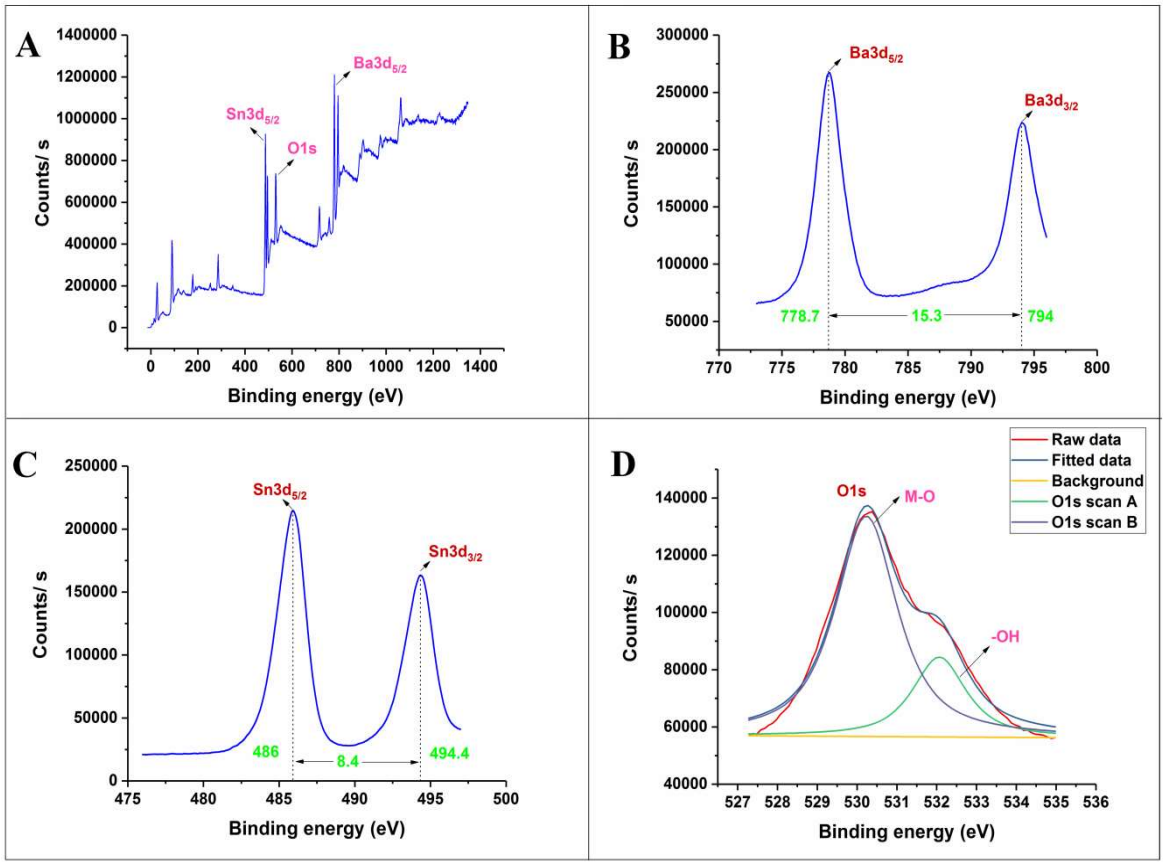

Figure 3.22 A) Wide XPS spectra of BSO catalyst calcined at 850°C, B) Ba3d spectra, C) Sn3d spectra, and D) deconvoluted O1s spectra of BSO catalyst

The intrinsic peaks in the wide XPS spectra of BSO (Figure 3.22A) suggested Ba, Sn and O elements were present in the catalyst. The oxidation state of the individual elements was confirmed by analyzing their core level spectrum. Figure 3.22B is displayed the 3d spectrum of barium (Ba) which indicates two sharp peaks at the

binding energy (B.E.) of 778.7 eV and 794 eV, which correspond to the spin orbit doublet $Ba3d_{5/2}$ and $Ba3d_{3/2}$ respectively. The definite difference of 15.3 eV between these two peaks has confirmed the +2 oxidation state of Ba (Miot et al., 1998). Figure 3.22C which is the 3d spectrum of tin (Sn) yielded two peaks correspond to the spin orbit doublet $Sn3d_{5/2}$ and $Sn3d_{3/2}$ at the B.E. of 486 eV and 494.4 eV respectively. The peak difference of 8.4 eV between two spin states suggested the presence of Sn^{4+} in BSO (Liu et al., 2017). The deconvoluted 1s spectra of oxygen (Figure 3.22D) has implied presence of two type of oxygen species in BSO. The lower B.E. of 530 eV corresponded to the fully coordinated oxygen of metal oxide; whereas, comparatively higher B.E. of 532 eV was assigned for O-H oxygen which came due to moisture contamination (John et al., 2019). Hence, the XPS analysis invariably justified the XRD result that BSO was existed in pure form of $BaSnO_3$ that constituted by Ba^{2+}, Sn^{4+} and O^{2-}.

3.7.4 SEM – EDAX analysis

The surface topology of pure SnO_2 and the synthesized catalysts was seen by scanning electron microscope (SEM). In Figure 3.23A, it is clearly viewed that SnO_2 particles were smaller in size and existed in agglomerated form. The SEM image of uncalcined BSO in Figure 3.23B comprises of fully agglomerated mixed phases of $Sn(OH)_2$ and $Ba(NO)_3$. After calcination at 850^oC, BSO showed smooth texture in morphology (see Figure 3.23C). The particles of BSO are seemed quite large and irregular in shape as compared to pure SnO_2.

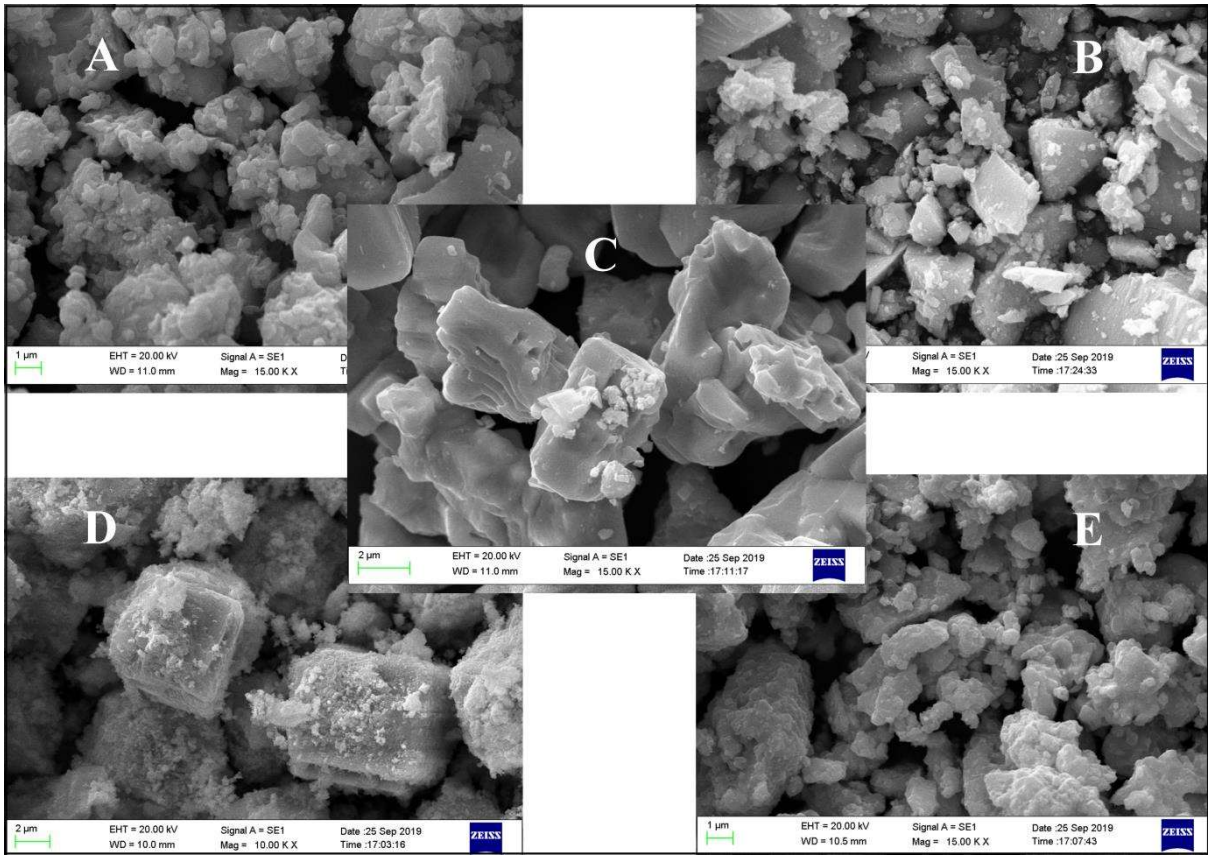

Figure 3.23 SEM image of A) pure SnO_2 B) uncalcined BSO catalyst C) calcined BSO catalyst D) calcined 2BSO catalyst E) calcined B2SO catalyst *

*all barium tin oxide catalysts were calcined at 850°C

In case of 2BSO (Ba/Sn 2 : 1) the SEM image (Figure 3.23D) displays scattered deposition of $BaCO_3$ over $BaSnO_3$. When the stoichiometric ratio of Sn was increased to 1 : 2, the excess tin formed its native oxide which introduced more heterogeneity in particle shape, size and texture. Figure 3.23E, the SEM of B2SO (Ba/Sn 1 : 2) implies that excess SnO_2 has randomly accommodated over the catalytic surface. The Ba/Sn atomic ratio of barium tin oxide catalysts was cross-verified by Energy-dispersive X-ray spectroscopy. Table 3.2 includes the atomic % and weight % of constituent atoms (Ba, Sn, O) present in catalysts. In the EDX spectra of BSO (shown in Figure 3.24), it was found that the atomic percentages of Ba, Sn and O were 19.51%,

21.25% and 59.24% respectively, which also implied that atomic percentage of Ba : Sn : O is 1 : 1 : 3. Thus, it can be stated that the $BaSnO_3$ was the only composition of catalyst BSO and this study supported the findings of XRD and XPS.

Table 3.2 Atomic percentage and weight percentage of barium tin oxide catalysts analyzed by EDAX

Sample name (Ba/Sn atomic ratio)	Atomic percentage (%)			Weight percentage (%)		
	Ba	**Sn**	**O**	**Ba**	**Sn**	**O**
Pure SnO_2	-	19.83	80.17	-	64.73	35.27
BSO (Ba/Sn 1:1)	19.51	21.25	59.24	43.58	41.01	15.41
2BSO (Ba/Sn 2:1)	21.20	11.14	67.66	54.77	24.87	20.36
B2SO (Ba/Sn 1:2)	10.77	22.71	66.52	26.18	56.12	17.70

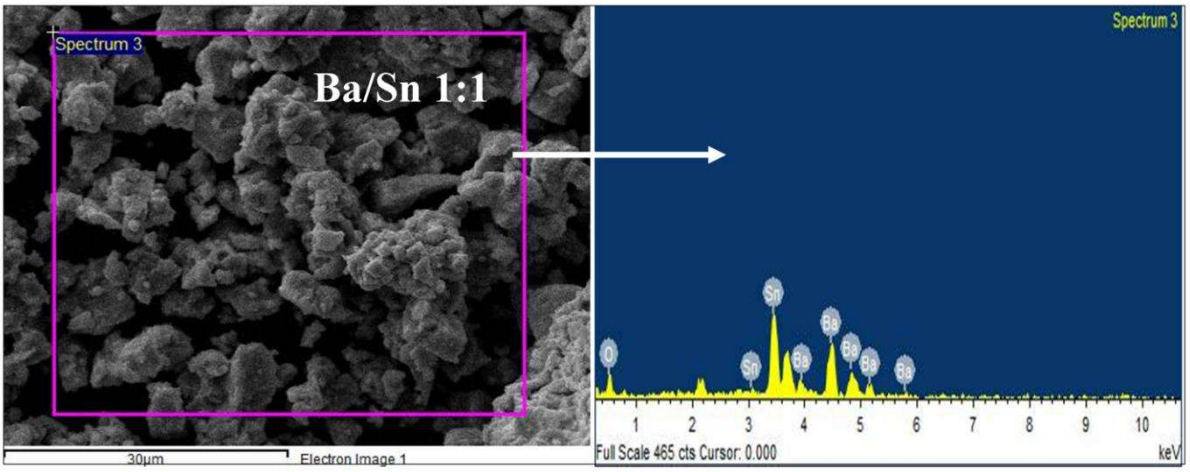

Figure 3.24 EDAX spectra of specified area of BSO catalyst

3.7.5 BET – BJH analysis

Surface area and basic strength of a catalyst have synergistic impact on transesterification reaction. Table 3.3 depicts the surface information including surface area, pore volume, and pore size of the barium stannate samples having different Ba/Sn atomic ratio. It was obtained that BET surface area of pure perovskite $BaSnO_3$ or BSO catalyst (Ba/Sn 1:1) was larger than that of other barium tin oxide catalysts like 2BSO, B2SO. It was also noticed that pore size distribution of the catalyst BSO was found in mesoporous range of 2-50 nm (Sahani et al., 2019) which is appreciable for base catalyzed transesterification reaction. The reason behind the lower surface area of 2BSO and B2SO may be the scattered distribution of the native oxides and carbonates of stoichiometrically excess components over the active surface of $BaSnO_3$. This justifications regarding BET analysis of the barium tin oxide catalysts have been deliberated by the mean of SEM images which show the topological view of such catalysts.

Table 3.3 Surface analysis of barium stannate compounds by BET - BJH

Sample	Surface area (m^2/g)	Pore volume (cm^3/g)	Pore diameter (nm)
BSO (Ba:Sn 1 : 1)	144.09	0.5578	28.34
2BSO (Ba:Sn 2 : 1)	26.88	0.0115	67.54
B2SO (Ba:Sn 1 : 2)	5.83	0.0069	58.03

3.7.6 Basicity analysis

The most important catalytic property i.e. basicity of catalyst samples (SnO_2, BSO, 2BSO and B2SO) were rationalised by Hammett indicator benzene carboxylic acid titration method. The total basicity of the catalysts were calculated by adding the individual

basicity found at three different pK_a values (i.e. 8.9, 9.3 and 15), derived by different indicators as thymol blue, phenolphthalein, and 2,4-dinitroaniline. Pure SnO_2 showed nil basic strength, whereas, BSO, 2BSO and B2SO catalysts had basic strength of 1.44, 0.87, 0.64 mmol/g respectively in the range of 8.9 < H_> 15.4. Such results clearly imply that pure SnO_2 had no basic site to interact with reactants but barium tin oxide catalysts had the appreciable basicity to act as efficient heterogeneous catalyst in transesterification reaction. In comparison, BSO had the highest basic strength, whereas excessive presence of carbonate species in 2BSO and SnO_2 in B2SO lowered the basic strength to greater extent. This happened due to acidic nature of both carbonate and SnO_2 reduced the basicity of the respective catalysts (Xie et al., 2011). Moreover, it is anticipated that the basic Ba-O bond in $BaSnO_3$ may play as active sites for probable interaction with triglyceride molecule.

3.8 Conclusions

This chapter introduced synthesis methods and characterizations of three new heterogeneous base catalysts for biodiesel production. Potassium modified ceria oxide (K-mod CeO_2), potassium tin oxide (KSO) and barium tin oxide (BSO) catalysts were synthesized via sol-gel auto combustion process, polymer precursor auto combustion process and wet impregnation process respectively. The thermal stability of the catalysts were investigated by TGA-DTA, revealed that K-mod CeO_2, KSO, and BSO catalysts were thermally stabilized at 739°C, 765°C, and 758°C respectively. The powder XRD confirmed the chemical phases present in catalysts calcined at different calcination temperatures. In case of K mod CeO_2, it was found that when the catalyst was calcined below 800°C, cerium was present in form of Ce_2O_3 along with $Ce(OH)_3$; however, when it was calcined at 800°C, cerium existed as CeO_2. The potassium species were accommodated at the interstitial points of the cerium oxide lattice, and it was confirmed

by the XRD data. In KSO, it was observed that in catalysts calcined at 500, 600 and 700°C, the metals (K and Sn) existed in their individual native oxide forms, but in the catalyst calcined at 800°C, metals formed three distinct compound phases as K_2SnO_3, $K_2Sn_2O_3$, and $K_2Sn_3O_7$. The XRD of barium tin oxide catalysts were quite interesting. The XRD of BSO (having Ba:Sn atomic ratio 1:1) revealed the single phase formation of $BaSnO_3$, however, in XRD of 2BSO (Ba:Sn = 2:1) and B2SO (Ba:Sn = 1:2) depicted that chemically excess Ba and Sn were present in $BaCO_3$ and SnO_2 along with $BaSnO_3$ in 2BSO and B2SO respectively. The oxidation state of each individual species present in catalysts was identified by XPS analysis, and the resultant XPS data was cross verified by XRD of the same. Morphological interpretation was delivered by SEM-EDAX analysis. It was found that the small sized rod shaped pure ceria oxide particles were transformed into large sized spherical particles after modification. However, in case of KSO 800 catalyst (calcined at 800°C), three different types of particles were found. Further EDAX confirmed that K_2SnO_3 possessed solid block like structure, $K_2Sn_2O_3$ particles were small sized spherical shaped agglomerated topology, and $K_2Sn_3O_7$ particles were needle shaped morphology. Comparing the SEM images of different barium tin oxide catalysts, it was confirmed that chemically excess $BaCO_3$ and SnO_2 were heterogeneous agglomerated over the surface of $BaSnO_3$ particles in 2BSO and B2SO respectively. BET surface area and basicity of the catalysts were investigated to predict the activity of such catalysts. After modification the surface area of the ceria oxide reduced due to increase the particle size, but the basicity increased due to incorporation of alkaline potassium species into the ceria matrix. In case of KSO catalyst, both the surface area and the basicity of the KSO 800 were obtained to be greater than that of other potassium tin oxides as the particles of KSO 800 were in less agglomeration and had particular shape and size, moreover KSO didn't contain the acidic carbonate species; thus, the basic property wasn't hampered.

Similarly, the surface properties of BSO were found to be far better than 2BSO and B2SO for the same reason as mentioned in KSO catalysts. In addition, the basic strength of 2BSO and B2SO were observed to be quite low than that of BSO. This happened due to both carbonate and tin oxide possessed acidic character that lowered the basic strength of the respective catalysts.